JOURNAL OF GEOPHYSICAL RESEARCH, VOL. 108, NO. D19, 4606, doi:10.1029/2002JD002987, 2003

Injection of gases into the stratosphere by explosive volcanic eruptions

Christiane Textor,[1] Hans-F. Graf, and Michael Herzog[2]
Max-Planck-Institut für Meteorologie, Hamburg, Germany

J. M. Oberhuber
Deutsches Klimarechenzentrum GmbH, Hamburg, Germany

Received 27 September 2002; revised 4 April 2003; accepted 25 April 2003; published 9 October 2003.

[1] Explosive eruptions can inject large amounts of volcanic gases into the stratosphere. These gases may be scavenged by hydrometeors within the eruption column, and high uncertainties remain regarding the proportion of volcanic gases, which eventually reach the stratosphere. These are caused by the difficulties of directly sampling explosive volcanic eruption columns and by the lack of laboratory studies in the extreme parameter regime characterizing them. Using the nonhydrostatic nonsteady state plume model Active Tracer High Resolution Atmospheric Model (ATHAM), we simulated an explosive volcanic eruption. We examined the scavenging efficiency for the climatically relevant gases within the eruption column. The low concentration of water in the plume results in the formation of relatively dry aggregates. More than 99% of these are frozen because of their fast ascent to low-temperature regions. Consideration of the salinity effect increases the amount of liquid water by one order of magnitude, but the ice phase is still highly dominant. Consequently, the scavenging efficiency for HCl is very low, and only 1% is dissolved in liquid water. However, scavenging by ice particles via direct gas incorporation during diffusional growth is a significant process. The salinity effect increases the total scavenging efficiency for HCl from about 50% to about 90%. The sulfur-containing gases SO_2 and H_2S are only slightly soluble in liquid water; however, these gases are incorporated into ice particles with an efficiency of 10 to 30%. Despite scavenging, more than 25% of the HCl and 80% of the sulfur gases reach the stratosphere because most of the particles containing these species are lifted there. Sedimentation of the particles would remove the volcanic gases from the stratosphere. Hence the final quantity of volcanic gases injected in a particular eruption depends on the fate of the particles containing them, which is in turn dependent on the volcanic and environmental conditions. *INDEX TERMS:* 0322 Atmospheric Composition and Structure: Constituent sources and sinks; 1610 Global Change: Atmosphere (0315, 0325); 3210 Mathematical Geophysics: Modeling; 3314 Meteorology and Atmospheric Dynamics: Convective processes; 8409 Volcanology: Atmospheric effects (0370); *KEYWORDS:* processes in the eruption column, scavenging of volcanic gases (SO_2, H_2S, HCl), stratospheric aerosol, climate impact of volcanoes, stratospheric chlorine

Citation: Textor, C., H.-F. Graf, M. Herzog, and J. M. Oberhuber, Injection of gases into the stratosphere by explosive volcanic eruptions, *J. Geophys. Res.*, *108*(D19), 4606, doi:10.1029/2002JD002987, 2003.

1. Introduction

[2] Volcanoes can inject large quantities of gases and particles into the stratosphere. At least once every 2 years, an eruption column penetrates the tropopause [*Simkin*, 1993]. Highly explosive volcanic events, like Pinatubo in 1991, affect the climate on time scales of months to years [e.g., *McCormick et al.*, 1995]. Mainly sulfur-containing volcanic gases are responsible for the climate effects of explosive volcanic eruptions. The oxidation of sulfur dioxide (SO_2) and hydrogen sulfide (H_2S) gases generates submicron sulfate particles with lifetimes of several years, which are radiatively active. Furthermore, the stratospheric ozone concentration is influenced: for the low chlorine loadings of the preindustrial period, it is expected to increase because volcanic sulfate aerosols cause a decrease of active nitrogen oxides, which destroy ozone under undisturbed conditions [*Brasseur et al.*, 1990; *Tie and Brasseur*, 1995]. After recent large volcanic eruptions,

[1]Now at Laboratoire des Sciences du Climat et de l'Environnement, L'Orme des Merisiers, Gif-sur-Yvette, France.
[2]Now at Department of Atmospheric, Oceanic and Space Sciences, University of Michigan, Ann Arbor, Michigan, USA.

Copyright 2003 by the American Geophysical Union.
0148-0227/03/2002JD002987

however, observations show a substantial depletion of stratospheric ozone. This has been explained by heterogeneous reactions at volcanic sulfate aerosols converting passive halogen compounds into active ones, which destroy ozone [e.g., *Hofmann and Solomon*, 1989; *Granier and Brasseur*, 1992; *Solomon et al.*, 1996]. Hence ozone depletion after explosive eruptions is only possible in the presence of chlorine, which is mainly caused by anthropogenic emissions of chlorofluorocarbons. The column ozone reduction attributed to the 1991 Mt. Pinatubo eruption ranged from about 2% in the tropics to about 7% in midlatitudes [*Angell*, 1997; *Solomon et al.*, 1998]. These ozone changes are a combined effect of perturbations in heating and photolysis rates, and in stratospheric chemistry. Ozone reduction may be strongly enhanced by an additional direct volcanic injection of hydrogen chloride (HCl).

[3] The composition of volcanic gases varies widely between volcanoes and is also dependent on the individual volcano's state of activity [e.g., *Symonds et al.*, 1994]. Sulfur gases contribute typically in the order of 1 to 25% by volume to the total gaseous eruptions. The dominant sulfur components are SO_2 and H_2S. The estimated mass of erupted SO_2 for the eruption of Mt. Pinatubo in 1991 was 14–26 Mt, 12–15 Mt, and 14 Mt as obtained from the Total Ozone Mapping Spectrometer (TOMS), Solar Backscatter Ultraviolet Instrument (SBUV), and Advanced Very High Resolution Radiometer (AVHRR) data, respectively [*Krueger et al.*, 1995]. The petrologic method (comparison of magmatic gas content in pre-eruptive and posteruptive gas inclusions) predicts a stratospheric release of only 0.22 Mt SO_2 [*Westrich and Gerlach*, 1992], but the authors doubt that this reflects the real total amount. The excess sulfur found in the satellite data is explained by a separate SO_2-rich fluid phase, which coexists with the magma [*Gerlach et al.*, 1996].

[4] The H_2S fraction in magma increases with increasing pressure (i.e., with depth of the magma chamber) and with decreasing temperature and oxygen concentration of the magma [*Gerlach and Casadevall*, 1986]. Satellite data of H_2S after explosive eruptions are not available because it cannot be detected by the systems in use at the moment. Petrological studies suggest that most of the sulfur gases in the 1982 El Chichón eruption was in the form of H_2S [*Rye et al.*, 1984; *Luhr et al.*, 1984]. Direct measurements of the posteruptive fumarolic activity, taken by *Kotra et al.* [1983] seven months after the main eruption, indicated a H_2S to total gaseous sulfur ratio of 80% by mass. The chemistry of H_2S in the stratosphere is discussed by *McKeen et al.* [1984]. H_2S is oxidized to SO_2 with an average lifetime of three days.

[5] An increase of stratospheric SO_2 on the second day after the end of eruption has been detected by the TOMS instrument for several explosive volcanic eruptions [*Bluth et al.*, 1995], e.g., for El Chichón [*Schneider et al.*, 1999]. However, no such posteruptive maximum was retrieved for Pinatubo [*Bluth et al.*, 1992]. The additional SO_2 is believed to be produced by oxidation of coemitted H_2S, which cannot be detected by the TOMS instrument [*Rose et al.*, 2000]. Thermodynamic calculations confirm this theory since they indicate a predominance of H_2S for the El Chichón eruption [*Rye et al.*, 1984; *Luhr et al.*, 1984] and of SO_2 for that of Pinatubo [*Westrich and Gerlach*, 1992]. The release of SO_2 from ice particles, in which it has been incorporated during plume rise, is discussed as another reason for the posteruptive stratospheric increase [*Rose et al.*, 2001]. Indications of ice in volcanic plumes were found in the eruption columns of Redoubt in 1989–90 [*Schneider and Rose*, 1994], Rabaul in 1994 [*Rose et al.*, 1995] and Soufrière Hills Volcano, Montserrat in 1998–99 [*Mayberry et al.*, 2001], Hekla in February 2000 [*Rose et al.*, 2000; *Krotkov and Krueger*, 2000], and Mt. Spurr in 1992 [*Rose et al.*, 2001]. Unusually low concentrations of SO_2 together with high ice concentration are suggestive of gas scavenging by ice particles [*Rose et al.*, 1995, 2001]. The stability of these particles, which can subsequently release SO_2 to the stratosphere, is dependent on the injection of water during the eruption, which is, in turn, dependent on the volcanic and environmental conditions [e.g., *Glaze et al.*, 1997].

[6] The main halogen component of volcanic emissions is HCl with 1 to 10% by volume [e.g., *Symonds et al.*, 1988]. Recently, significant amounts of Bromine were found in volcanic ash [*Sachs and Harms*, 2000; *Bureau et al.*, 2000]. The eruption of El Chichón in 1982 released approximately 1.8 Mt HCl as derived from the petrological method [*Varekamp et al.*, 1984]. About one month after the main eruption, halite (NaCl) particles have been observed in the stratospheric aerosol cloud. These vanished after three months, possibly through conversion to HCl, via the reaction with H_2SO_4 [*Woods et al.*, 1985]. Three months after the main eruption, when the volcanic cloud had zonally circled the globe extending from 10°S to 35°N in latitude, *Mankin and Coffey* [1984] determined an HCl total column content inside this cloud, which was about 40% higher than the background value. The observed increase in HCl may be due to a direct injection of chlorine into the stratosphere. During the eruption of Mt. Pinatubo, *Westrich and Gerlach* [1992] estimated an emission of about 4.5 Mt HCl, derived from the petrological method. However, no substantial HCl increase was detected in the stratosphere in the weeks that followed the eruption [*Mankin et al.*, 1992; *Wallace and Livingston*, 1992]. This discrepancy indicates significant removal of HCl in the Pinatubo eruption column before it could enter the stratosphere. The observed enhancement of chlorine dioxide (OClO) associated with the volcanic cloud is explained by heterogeneous reactions at volcanic sulfate aerosols, which transferred nonvolcanic HCl to OClO [see, e.g., *Solomon et al.*, 1993; *Waters et al.*, 1993; *Toohey et al.*, 1993].

[7] Until recently, no HCl increase was detected in ice core data, not even after the biggest volcanic events, which are accompanied by a strong sulfate signal [e.g., *Delmas*, 1986; *Holdsworth et al.*, 1986]. However, *Wagnon et al.* [1999] found evidence for a strong HCl signal in Antarctica from an eruption in 1259. The authors argue that the increase of acidity caused by the deposition of volcanic sulfuric acid leads to a decrease of the ice-solubility of other acidic species, so that these will be expelled to the gaseous phase. Hence HCl cannot be found in the same layer as sulfate but in adjacent, less acidic ones. *Zdanowicz et al.* [1999] found a strong volcanic chlorine peak in the GISP2 Greenland ice core, which was attributed to the eruption of Mount Mazama 7627 ± 150 years before present. The authors calculated a maximum stratospheric loading of

8.1 Mt Chlorine, which is two orders of magnitude lower than the value derived from a petrological analysis of Mount Mazama melt inclusions [*Bacon et al.*, 1992], again suggesting HCl removal within the eruption column.

[8] The determination of gas concentrations within a volcanic plume is extremely difficult because of the inherent health risks, and because of the cloud opacity. Ash deposits of historical eruptions can be examined with the petrological method. Volcanic emissions are observed in situ with ground-based, airborne, and satellite remote sensing instruments. The employment of the latter is the most comprehensive way to measure volcanic eruption clouds for the time being. However, the results are affected by the high optical depth of the plume and the reflectivity of the underlying surface. In addition, the errors vary with cloud mass and area, and they depend on the quality of the estimation of the plume's trajectory and dilution. For example, the error of the total SO_2 mass retrieved from TOMS data ranged from 15 to 30% [*Krueger et al.*, 1995]. The results from different methods often diverge by orders of magnitude. The enormous discrepancies of the data are due to the inaccuracies of each individual measuring technique, but they also result from the fact that the eruption cloud is investigated at different distances from the crater, and during different states of the eruption. High uncertainties remain regarding the proportion of volcanic gases, that eventually reach the stratosphere, in particular for historic eruptions.

[9] The fraction of volcanic gases injected into the stratosphere was investigated through numerical simulations by *Tabazadeh and Turco* [1993] with the one dimensional, steady state plume model of *Woods* [1988]. Complex thermodynamic theory was applied to estimate the scavenging efficiency. The authors pointed out that HCl is almost completely transferred into supercooled drops, resulting in an HCl vapor pressure reduction of up to four orders of magnitude. On the other hand, it was found that the scavenging of SO_2 in the eruption column is insignificant. Owing to its low solubility in liquid water, this gas reaches the stratosphere almost unaffected by scavenging in the plume. The study of *Tabazadeh and Turco* [1993] stands as an important first attempt to simulate the physical chemistry in an eruption of Plinian type. (These eruptions are highly explosive with high columns resulting from high-velocity, voluminous, gas-rich eruptions.) However, their simulations were based on a relatively simple treatment of the dynamics. They did not consider cloud microphysical processes, such as precipitation or ash aggregation. All hydrometeors were liquid, and incorporation of gases in ice particles was not included. However, as we will show later, the formation of ice can significantly alter the gas scavenging efficiency in the plume.

[10] The fate of volcanic gases in the plume is determined by scavenging or chemical processes. Prior to this study, we examined the potential of photochemical reactions to change volcanic gas concentrations within an ascending explosive eruption column. We performed sensitivity studies with a chemistry box model, which included reactions in the gas and in the liquid phase, under volcanic conditions. These simulations indicate that photochemistry can be neglected because it is strongly suppressed by the high optical depth of the ash cloud. Even in the outer regions of the plume, which are less dense, the surplus of reduced compounds, like SO_2 or H_2S, depletes oxidizing species, this way disrupting radical chemistry. In addition, the characteristic times of the relevant reactions are greater than the time to rise from the crater to the stratosphere, which is less 10 min. Thus scavenging by hydrometeors and hydrometeor-ash aggregates is the dominant process modifying volcanic gas concentrations within the eruption column.

[11] The goal of this study is to identify the important processes governing gas scavenging efficiency, and the parameters controlling these processes. We have developed a comprehensive numerical model, which for the first time represents the significant dynamical, microphysical, and chemical processes in volcanic eruption columns. Using this model, we examine the factors which determine the proportion of the climatically most relevant volcanic gases (HCl, SO_2 and H_2S) that eventually reach the stratosphere.

[12] In the first part of this paper we describe the plume model, and the parameterizations developed to describe gas scavenging processes by liquid water and ice. In the second part, we present numerical experiments investigating the parameters, which govern the scavenging efficiency and the injection of volcanic gases into the stratosphere.

2. Plume Model ATHAM

[13] The nonsteady state, nonhydrostatic numerical model Active Tracer High Resolution Atmospheric Model (ATHAM) is designed to simulate the dispersal of explosive volcanic eruption columns in the atmosphere. The model has been employed to examine the effects of different environmental conditions on the plume development [*Herzog et al.*, 1998; *Graf et al.*, 1999]. A special feature of ATHAM is its ability to consider the contribution of individual tracers to the mean density and heat capacity of the gas-particle mixture. Thus these so-called active tracers, like volcanic ash which occurs in a very high concentration, can influence the dynamics of the multicomponent system. A large set of equations is necessary to describe the dynamics and thermodynamics of each component, and the interactions between them. For a high number of active tracers, the solution of this set is only feasible with additional simplifications: on the condition that all particles are small, the assumptions of thermal and dynamical equilibria are valid, and the equations can be solved for volume mean quantities only. (In thermal equilibrium, all tracers have the same in situ temperature. In dynamical equilibrium, accelerations between solid or liquid tracers and the surrounding gas do not exist, and tracers move with their terminal fall velocity. However, the mixture can be accelerated as a whole.) In this way, the number of prognostic quantities is strongly reduced. The dynamical behavior of the gas-particle mixture is described by five prognostic equations for the three momentum components, the pressure, and the temperature. Active tracers and dynamical variables are coupled via the bulk density and the heat capacity of the mixture. For each active tracer, one additional transport equation is taken into account. Different tracers can have different fall velocities.

[14] In the high-pressure regime in the conduit and at the vent, the condition of dynamic equilibrium is not fulfilled. Hence small scale processes in the high pressure and temperature regime near the crater are not resolved

within ATHAM. We focus on processes occurring in the eruption column, in the range of some tens of meters to some tens of kilometers. The simulations start after pressure adjustment to atmospheric values and last for a few hours. Typically, decompression takes place within a vertical distance of some column radii above the vent; thus we can neglect the topography of the volcanic crater and use a flat surface. Owing to the low gas content of the erupting gas-particle mixture, the temperature does not change significantly during decompression [*Woods and Bower*, 1995]. Therefore we can use temperature data obtained from thermochemical calculations to initialize the model. The vertical velocity after decompression at the base of the eruption is about twice the speed of sound in the gas-particle mixture [*Woods and Bower*, 1995]. To prescribe the volcanic forcing in ATHAM, we choose a composition and temperature of the erupting mixture, and its mass eruption rate. From these values, we can compute the vertical velocity and the radius of the base of the eruption column.

[15] Cloud microphysics is parameterized according to the concept of *Walko et al.* [1995] and *Meyers et al.* [1997]. In this bulk two-moment scheme, the mass mixing ratio and the number concentration of the particles are predicted. We consider liquid and frozen hydrometeors, and the feedback of latent heat release on the plume dynamics. Our parameterization includes the interaction of hydrometeors and volcanic ash, taking into account the condensation of hydrometeors on ash particles. As soon as the ash particles are coated with water or ice, they are allowed to aggregate with the hydrometeors acting as adhesive, this way forming larger hydrometeor-ash aggregates. Thus in ATHAM aggregation of ash is due to gravitational capture of ash particles of different size, in the presence of water or ice, and we simulate the formation of accretionary lapilly. (Accretionary lapilly are spherical aggregates with sizes between 2 and 64 mm. They form when ash particles carrying a film of water collide and stick together.) The aggregation coefficients (describing the ratio of the number of collisions leading to particle growth to that of all collisions) are obtained from cloud the microphysical literature for the coagulation of different sized hydrometeors [see, e.g., *Pruppacher and Klett*, 1997]. These coefficients are modified with a simple function depending on the amount of hydrometeors (water or ice) available at the particle. A schematic representation of the microphysical processes in ATHAM can be found in Figure 1, for a full description see *Textor* [1999] and C. Textor et al. (manuscripts in preparation, 2003).

[16] In this study we use the two dimensional, axisymmetric version of the plume model. This version is more economical in terms of computer memory and time. Cross winds, which exert a strong effect on the plume's shape and height [*Ernst et al.*, 1994; *Graf et al.*, 1999] cannot be studied. However, the dilution of the mixture by entrainment of surrounding air corresponds to a three dimensional simulation with an atmosphere initially at rest. For this study, ATHAM consists of five modules:

[17] 1. The dynamic part solves the Navier-Stokes equation for the gas-particle mixture, and includes the transport of active tracers [*Oberhuber et al.*, 1998; *Herzog*, 1998].

[18] 2. The turbulence closure scheme delivers the turbulent exchange coefficients for each dynamic quantity, thereby describing the entrainment of ambient air into the plume [*Oberhuber et al.*, 1998; *Herzog et al.*, 2003].

[19] 3. The cloud microphysics describes condensation of water vapor and formation of precipitation. All phases of water are included: vapor, liquid and solid. The feedback of the thermal energy changes on the dynamics is considered [*Textor*, 1999; C. Textor et al., manuscripts in preparation, 2003].

[20] 4. The aggregation module describes particle growth and coagulation based on microphysical interactions between hydrometeors and ash [*Textor*, 1999; C. Textor et al., manuscripts in preparation, 2003].

[21] 5. The scavenging module calculates dissolution of volcanic gases into drops, and the incorporation of volatiles into ice particles. The redistribution of gases contained in hydrometeors due to microphysical processes is included [*Textor*, 1999; *Textor et al.*, 2003; this paper].

[22] For a complete description of the model, see the above cited literature. The parameterization used in the scavenging module is described in the following section.

3. Parameterization of Gas Scavenging

3.1. Scavenging of Gases by Liquid Water

[23] The solubility of a gas in liquid water is described by the effective Henry law coefficient *He**. This coefficient describes the solubility of a gas in water including the chemical equilibrium due to acid dissociation, which enhances the uptake of gases in drops, for a review see *Sander* [1999]. The solubility of acid gases decreases with increasing acidity of the aqueous phase, and it decreases exponentially with increasing temperature as given by the van't Hoff equation [e.g., *Atkins*, 1986]. The solubility of HCl is about four orders of magnitude higher than that of SO_2 or H_2S. HCl is likely to be completely scavenged by water drops; its revolatilization would require a drastic decrease of the system's liquid water content.

[24] In this study, the time-dependent phase transfer of volcanic volatiles from the gas phase into drops is parameterized using the approach of *Schwartz* [1986]. The phase transfer rate of volatiles into liquid drops is proportional to the deviation from the solubility equilibrium:

$$\frac{\partial}{\partial t} c_{aq} = -\frac{1}{L}\frac{\partial}{\partial t} c_g = k_t \left(c_{g,\infty} - c_{g,eq}\right), \qquad (1)$$

where c_{aq} is the total aqueous concentration including dissociation products. $c_{g,eq}$ denotes the concentration in the gas phase at the drops' surface, given by the effective Henry law constant. $c_{g,\infty}$ is the gaseous concentration in the undisturbed environment, and L is the liquid water content in $kg_{aq}/kg_{totalmass}$. (The index "total mass" refers to the sum of the masses of all tracers in a grid cell.) Concentrations c are given in $mol/kg_{totalmass}$. The phase transfer constant k_t in s^{-1}, applies both for dissolving and degassing. It is defined as the reverse sum of the characteristic times for the gas mass transport to the drop surface, τ_{dg}, and across the air-water interface, τ_i (including the possible establishment of

solubility equilibrium locally at the interface) [*Schwartz*, 1986]:

$$k_t = \left(\tau_{dg} + \tau_i\right)^{-1} = \left(\frac{r^2}{3D_g^*} + \frac{4r}{3\overline{\upsilon}\alpha_{aq}}\right)^{-1}, \tag{2}$$

$$\text{where} \quad D_g^* = \lambda\overline{v}\left(1 + 0.22\,Re^{1/2}\right)$$
$$\text{and} \qquad \overline{v} = \sqrt{\frac{8RT}{M\pi}}. \tag{3}$$

r is the volume mean radius of the particle, in m. D_g^* is the gas phase diffusion coefficient, in m^2/s, including the effects of turbulence caused by circulation around a falling drop, Re is the Reynolds number. $\overline{\upsilon}$ denotes the mean speed of gas molecules derived from the kinetic gas theory, in m/s. R = 8.3143 mol/KJ is the general gas constant. M, in kg/mol, is the molecular weight, and λ, in m, the mean free path in air. The mass accommodation (or sticking) coefficients $\alpha_{aq\mathrm{HCl}}$ = 0.2 and $\alpha_{aq\mathrm{SO_2}}$ = 0.11 are taken from *DeMore et al.* [1997]. The value for H_2S is estimated ($\alpha_{aq\ \mathrm{H_2S}}$ = 0.1) to be in the range of the other values because no observational data are available.

[25] The resulting set of stiff nonlinear equations is solved with an implicit time stepping procedure employing Newton's method [*Press et al.*, 1992]. The Jacobian matrix is iteratively solved with a very efficient realization of a Gauss elimination.

3.2. Scavenging of Gases by Ice

[26] The solubility of gases in ice is much lower than in liquid water since solutes are rejected by the ice matrix. However, field studies [e.g., *Voisin et al.*, 2000; *Laj et al.*, 2001], a number of laboratory experiments (for reference, see, e.g., *Diehl et al.* [1998]), and numerical simulations [e.g., *Mari et al.*, 2000] indicated that gaseous species are scavenged by ice particles in the atmosphere. Their concentration in the ice phase often does not correspond to the thermodynamic equilibrium solubility, but is rather governed by condensation kinetics. This is caused by the low diffusivities of most electrolytes in ice, which prevent species once incorporated to considerably change their position within the ice crystal lattice. Field studies in Greenland showed that the concentration of HCl in snow was about one order of magnitude lower than the equilibrium value [e.g., *Dominé et al.*, 1995]. *Dominé and Thibert* [1996] and *Thibert and Dominé* [1997] assumed that ice particles can also trap amounts of HCl above the equilibrium saturation limit, e.g., in polar stratospheric clouds. This could also happen in volcanic clouds, where high gas concentrations and together with rapid ice growth occur.

[27] The gas uptake efficiency has been investigated by a number of laboratory studies [e.g., *Sommerfeld and Lamb*, 1986; *Valdez et al.*, 1987; *Valdez and Dawson*, 1989; *Clapsaddle and Lamb*,1989; *Mitra et al.*, 1990; *Conklin and Bales*, 1993; *Conklin et al.*, 1993; *Diehl et al.*, 1995; *Santachiara et al.*, 1995; *Dominé et al.*, 1995; *Dominé and Thibert*, 1996; *Santachiara et al.*, 1998; *Diehl et al.*, 1998; *Huthwelker et al.*, 2001]. It is a function of the gaseous species' partial pressure, its mass accommodation coefficient, its solubility and diffusivity in ice. In addition, the crystalline structure and growth rate of the ice particles play an important role [e.g., *Pruppacher and Klett*, 1997]. The gas uptake efficiency also depends on the quality of the ice surface. Its disordered structure has lead to the imagination of a quasi-liquid layer [*Faraday*, 1859], but great uncertainties remain regarding its characteristics [e.g., *Pruppacher and Klett*, 1997]. Gas uptake is also influenced by the presence of additional substances in the gas and in the ice phase.

[28] The mass of the incorporated species is roughly proportional to the mass of water vapor converted to ice. *Dominé et al.* [1995], and *Dominé and Thibert* [1996] suggested that the species concentration in ice is determined by the ratio of the number of molecules n_c to that of n_{H_2O} that hit and stick to the ice surface. The parameterization of gas scavenging by ice particles in ATHAM is based on this kinetic approach: the rate of incorporation of a chemical species c into ice crystals is proportional to the amount of water vapor q deposited, which is calculated in the microphysical module:

$$\frac{\partial}{\partial t}c_i = -\frac{\partial}{\partial t}c_g = -\frac{\partial}{\partial t}q_g\,\frac{c_g}{q_g}\,\frac{\alpha_{ic}}{\alpha_{i\,H_2O}}\,\sqrt{\frac{M_{H_2O}}{M_c}}. \tag{4}$$

[29] The indices g and i refer to the gas and to the ice phase, respectively. The mass accommodation coefficient for HCl, $\alpha_{i\mathrm{HCl}}$ = 0.3, is taken from *DeMore et al.* [1997]. For SO_2 and H_2S we assume the same values as for liquid water, $\alpha_{i\mathrm{SO_2}}$ = 0.11 and $\alpha_{i\ \mathrm{H_2S}}$ = 0.1 because no observational data are available. For water vapor we use $\alpha_{i\ \mathrm{H_2O}}$ = 0.5 [*Haynes et al.*, 1992]. Hence for the same concentrations in the gas phase, water vapor will be most effectively incorporated into ice particles, followed by HCl, H_2S and SO_2.

[30] In the context of this work, we neglect any dependence of the mass accommodation coefficients on temperature or composition. Considering the poor data basis, we believe that this simplification is suitable for a first investigation of the significance of gas incorporation into ice particles in a volcanic eruption column. The sensitivity of the scavenging efficiency on variations of the mass accommodation coefficient is examined in section 5.3. *Santachiara et al.* [1998] found a saturation solubility for SO_2 in the ice phase. We perform a sensitivity study in section 5.3, where we set the maximum solubility in ice equal to that in liquid water, as given by Henry's law (see section 3.1).

3.3. Transfer of Solutes During Microphysical Processes

[31] Evaporation of liquid water drops increases the solution concentration, condensation of water vapor dilutes it. This leads to a transfer of chemical species across the phase boundary in order to reach the equilibrium solubility given by Henry's law. This process is described by equation (1). The species are released back to the gas phase upon total drop evaporation, and we neglect a possible aerosol formation due to the crystallization of salt particles.

[32] Gases incorporated in ice particles are partly released to the atmosphere during sublimation. In spite of

some laboratory experiments [see, e.g., *Diehl et al.*, 1995], the information about the degree of gas retention during this process is limited. In ATHAM, we assume complete release, i.e., a proportionality to the amount of sublimating water vapor. In accordance with equation (4) we get: %

$$-\frac{\partial}{\partial t}c_i = \frac{\partial}{\partial t}c_g = -\frac{\partial}{\partial t}q_i \frac{c_g}{q_g} \frac{\alpha_{iH_2O}}{\alpha_{ic}} \sqrt{\frac{M_c}{M_{H_2O}}}. \quad (5)$$

Microphysical processes converting condensed hydrometeors from one class to another lead to corresponding transfers of chemicals contained in these hydrometeors, and new drops or ice particles with average concentrations are generated. In ATHAM, we assume that the transfer rate of a chemical species is proportional to that of the hydrometeor class in which is it contained. We consider the sum of the microphysical processes affecting that particular hydrometeor type. The transfer rate is then given by:

$$\frac{\partial}{\partial t}c_y = \sum_{procs} \frac{c_y}{q_y} \left(\frac{\partial}{\partial t}q_y\right), \quad (6)$$

where c_y is the content of a chemical species in a hydrometeor class y, in $mol/kg_{totalmass}$, and q_y is the mass mixing ratio of this hydrometeor class, in $kg/kg_{totalmass}$. Equation (6) is applied for coalescence of liquid and frozen hydrometeors, and for freezing and melting. These latter two processes are discussed below.

[33] When an aqueous solution freezes, the solutes are partly segregated from the ice lattice, leading to a higher concentration in the remaining liquid. Volatile solutes may evaporate depending on their specific water solubility given by Henry's law. Various solid and liquid phases can exist in thermodynamic equilibrium, depending on temperature and solute concentration [e.g., *Levine*, 1995]. Complete solidification occurs only at the so-called eutectic temperature (see section 3.4). As mentioned in section 3.2, the equilibrium solubility of chemical species in ice is in general lower than in the liquid phase, but the actual concentration can be much higher. The retention coefficient describes the efficiency by which a species is retained in the ice matrix. It depends on ice growth modality, temperature, and the presence of additional species [see, e.g., *Voisin et al.*, 2000]. *Iribarne and Pyshnov* [1990] demonstrated that some highly soluble species, among them HCl, were almost completely transferred to the ice phase during shock freezing. For SO_2, retention coefficients between 10% and 74% have been observed [e.g., *Lamb and Blumenstein*, 1987; *Iribarne et al.*, 1983]. Retention increases with increasing freezing rate, hence for higher supercooling and smaller drops [*Iribarne et al.*, 1990], and with decreasing SO_2 gas concentration [*Santachiara et al.*, 1995]. In a volcanic eruption column, liquid drops freeze very rapidly because of their rapid ascent (about 100 m/s) to regions with very low temperatures. Hence chemical species in liquid drops are completely retained in the ice phase in ATHAM. In an analogous manner, we assume for the melting process that species contained in ice particles are completely transferred to the liquid phase.

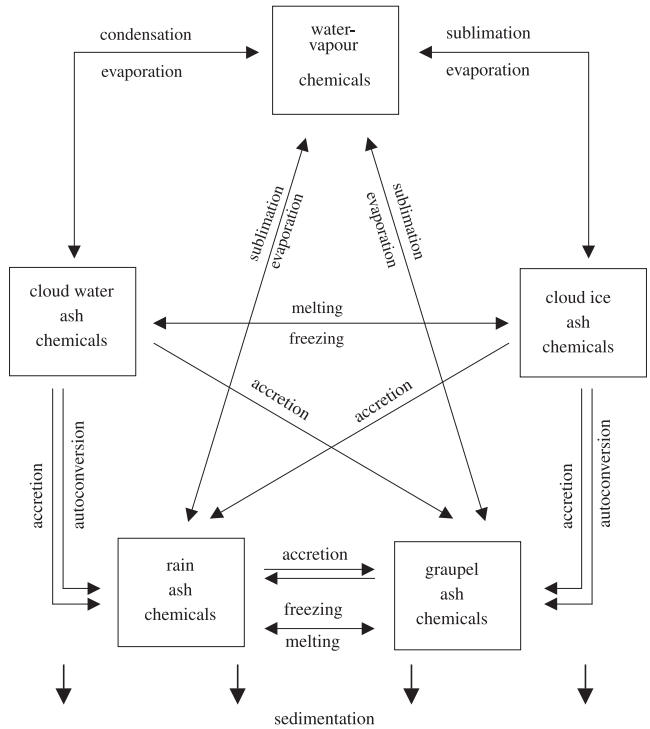

Figure 1. Scheme of the microphysical processes included in the scavenging module.

[34] The processes included in the scavenging module guarantee that volcanic species, initially erupted as gases, can be contained in each class of hydrometeor. Once scavenged, they experience the microphysical processes as shown in Figure 1.

3.4. Salinity Effects

[35] Solutes change the thermodynamic properties of water. The solution's saturation vapor pressure and freezing temperature is lowered [e.g., *Levine*, 1995]. In an ideal diluted solution, these effects are only dependent on the mole fraction, x, of the species, i, but not on the solute's chemical nature. According to Raoult's law, the saturation pressure of water vapor over an ideal dilute solution of a nonvolatile solute in water is given by:

$$p_{sat,l} = p^o_{sat,w} \cdot \left(1 - \sum_{i=1}^{n} x_i\right), \quad (7)$$

where $p^o_{sat,w}$ and $p_{sat,l}$ are the saturation vapor pressure of pure water and the solution, respectively. The freezing point depression of an ideal dilute solution is given by [e.g., *Levine*, 1995]:

$$T_f = T_f^0 - \left(T_f^0\right)^2 \frac{R}{\Delta H_f} \sum_{i=1}^{n} x_i = T_f^0 - k_f \sum_{i=1}^{n} x_i, \quad (8)$$

where $k_f = 103.27\ K$. $T_f^0 = 273.15\ K$ and T_f are the freezing point of pure water and the solution, respectively. R =

8.3143 *J/mol K* is the general gas constant and $\Delta H_f = 6007$ *J/mol* the molar enthalpy of freezing.

[36] In reality, even the binary system of HCl/H_2O does not behave like an ideal dilute solution. The freezing point depression for mole fractions of HCl greater than about 10^{-4} is much stronger than the ideal linear approach suggests [e.g., *Thibert and Dominé*, 1997]. HCl dissolves in ice and forms a solid solution up to the saturation solubility which depends on the temperature. For higher HCl concentrations, the solid solution of HCl in ice coexists with an aqueous solution, or with condensed crystalline hydrates of HCl, depending on HCl concentration and temperature. Liquid aqueous solutions are possible down to the eutectic temperature (198.45 K), when the solution completely solidifies. Recently, amorphous $HCl-H_2O$ solids have been observed at temperatures below 190 K [*Banham et al.*, 1996; *Dominé and Xueref*, 2001].

[37] In a volcanic eruption column, drops contain dissolved gases and salts of unknown qualities and quantities, see, e.g., *Mackinnon et al.* [1984], or *Smith et al.* [1982]. These multicomponent electrolyte solutions cannot be regarded as ideal because of the long-range interionic forces, that influence the actual concentrations, also called activity, a_i, of the solutes and of water. In real solutions a_i replaces the mole fraction, x_i, in equations (7) and (8). The activity can be larger or even smaller (due to the formation of ion pairs) than the ideal value with $a_i = x_i$. The properties of multicomponent solutions cannot be predicted a priori at any concentration, but have to be derived from simplified models which contain empirical parameters. Sophisticated thermodynamic theory treats intermolecular and interionic interactions in solutions in order to determine the solute activity [see, e.g., *Kim and Seinfeld*, 1993a, 1993b, *Carslaw et al.*, 1997].

[38] The water vapor saturation pressure over ice containing a solute can be substantially reduced, when compared to that over pure ice [e.g., *Chen and Crutzen*, 1994]. Nonideal effects and the possible presence of a quasi-liquid layer at the ice particles' surfaces complicates a comprehensive characterization of the saturation vapor pressure depression of ice containing solutes (see section 3.2).

[39] We investigate the impact of the salinity effect on gas scavenging in volcanic plumes, employing equations (7) and (8). Because of the major uncertainties concerning the composition of the hydrometeors and the concentrations involved, we believe that is it not possible to completely describe the real properties of the liquid and solid hydrometeors in a volcanic eruption column, not even with comprehensive thermodynamic models for multicomponent solutions. Hence we use simple parameterizations for the representation of the activities in order to assess the principal importance of the salinity effect in section 5.4.

4. Model Setup

[40] We simulate a typical highly explosive volcanic eruption [see, e.g., *Sparks et al.*, 1997] under subtropical atmospheric conditions. The experiments are performed on a stretched lattice with 150 × 80 grid points in cylindrical coordinates. The model domain is 300 km in the horizontal and 50 km in the vertical. In the center of the model domain, where the volcano is situated, the resolution is 250 m in the horizontal and 300 m in the vertical, at the lateral boundaries it is about 5 km. This grid choice allows for the plume dispersal without disturbances from the model boundaries during our simulation time of 90 min, with restricted computer resources. The volcanic forcing is specified by the vertical velocity, temperature, and composition of the erupted gas-particle mixture at three model grid points representing the base of the eruption column. The vertical velocity is increased to its maximum value within the first 60 s of the eruption. This value is maintained during the eruption period of 30 min, and reduced to zero during the last 3 min. We continue the experiment for additional 60 min in order to investigate the posteruptive development of the volcanic eruption cloud. Two classes of particles with mean radii of 2.5 and 50 μm are emitted, with the larger class contributing 60% by mass. We have fitted their size distributions to represent the ash fall data of the 1980 eruption of Mt. St. Helens [*Carey and Sigurdsson*, 1982]. The particle density is set to $\rho = 1800\ kg/m^3$.

[41] The chemical species are initialized in the concentration range typical for a Plinian eruption. Volcanic gas emissions are highly variable, and the concentrations of the sulfurous species are often higher than that of HCl. For this paper, however, we choose the same concentrations for all volatiles in order to simplify the comparison of their different behavior in the plume.

[42] In this paper the volcanic forcing and the ambient conditions are the same for all experiments. The volcanic conditions at the plume base are listed in the following. The height was 600 m above sea level, and the diameter 750 m. The vertical velocity was 400 m/s, and the temperature 1100 K. The mass mixing ratio of all gases was 7.34%. Water vapor contributed 81.74% by mass to this gas fraction. The gas ratios of HCl, SO_2 and H_2S were 0.1 $mol/kg_{totalmass}$ each (i.e., 1% by mass of the gas fraction). The density of the gas-particle mixture was 2.6 kg/m^3 and the mass eruption rate $4.5 \cdot 10^8$kg/s. For initializing the ambient temperature and humidity we use standard atmospheric profiles for the subtropics taken from *McClatchey et al.* [1972], with the tropopause at about 17 km as shown in Figure 2.

5. Results

[43] We present results from numerical experiments performed with the ATHAM model. All simulations include the sulfurous species SO_2 and H_2S. Both of these are only slightly soluble in liquid water, and their efficiency factors for incorporation into ice are similar. Hence we show results only for SO_2 here.

[44] In section 5.1 we describe the reference experiment, for which the general plume characteristics of tephra, hydrometeors and volcanic gases in the atmosphere are examined. (Tephra is a general term for fragments of volcanic rock and lava regardless of their size, that are erupted into the air.) Section 5.2 discusses the scavenging efficiency for HCl and SO_2 by liquid drops and ice particles in the plume, which control the injection of these gases into the stratosphere. We examine the impact of gas incorporation into ice in section 5.3, and the salinity effects in section 5.4.

5.1. General Characteristics of the Eruption Column

[45] In the reference experiment, the plume penetrates the tropopause at 17 km about 5 min after the eruption has

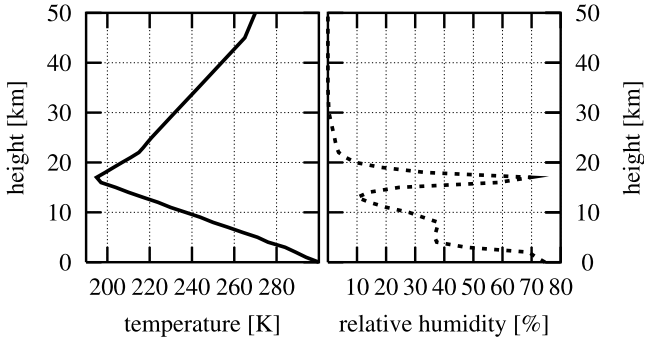

Figure 2. Atmospheric profiles for temperature and relative humidity.

started. The average vertical velocity in the core is greater than 100 m/s. The eruption column consisting of the hydrometeor-ash aggregates is shown 30 min after the eruption onset (Figure 3).

[46] The height of neutral buoyancy occurs at about 23 km, 6 km above the tropopause, and the eruption overshoots this height by more than 5 km. The ash fraction of hydrometeor-ash aggregates is typically greater than 80% by mass. (All fractions given in this paper are mass fractions if not otherwise noted.) This reflects the fact that the total mass of tephra in the model domain after 30 min is about 100 times that of hydrometeors. Hence Figure 3 corresponds roughly to the plume of pure volcanic ash. Figure 4 depicts the vertical distribution of ash at different times during the course of the simulation. The vertical ash distribution is the horizontal integral of ash at each height level. The larger particles (>50 μm in radius) settle into the troposphere, forming a distinct ash layer. This is indicated in Figure 4 by the lower peak in the distributions, which moves downward with time from the height of neutral buoyancy, which was reached after 5 min, to about 5 km after 90 min (i.e., one hour after the end of the eruption). The narrower, stationary peak at about 23 km stems from small particles (about 2.5 μm in radius), which are suspended within the umbrella region. This portion of the cloud spreads horizontally in the

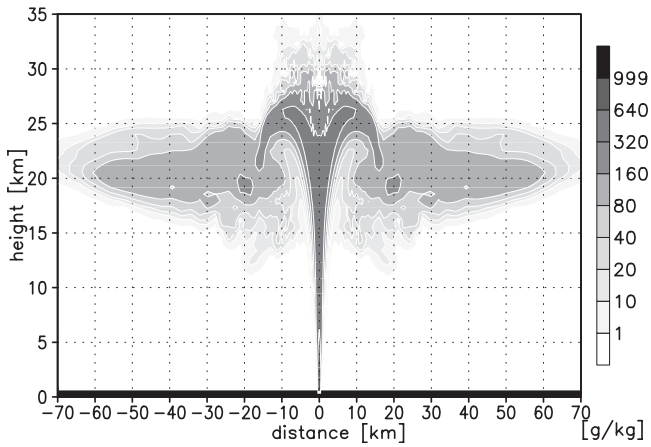

Figure 3. Eruption cloud of hydrometeor-ash aggregates, shown for the reference experiment after 30 min. The scale gives mass mixing ratio in $g/kg_{totalmass}$.

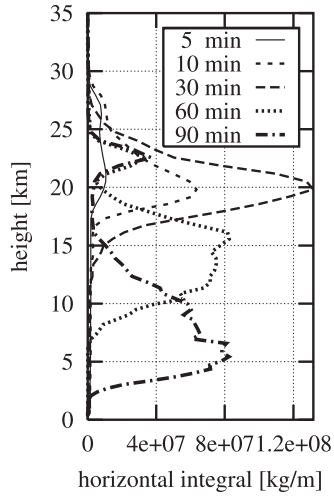

Figure 4. Vertical distribution of ash particles at t = 5, 10, 30, 60 and 90 min, shown for the reference experiment. The scale gives kg/m.

stratosphere. After 90 min, the plume has a horizontal extend of about 250 km, and only about 10% of the erupted ash can be found in the stratosphere.

[47] Figure 5 shows the temperature distribution in the eruption column after 30 min. At this time, temperature ranges from 1100 K at the vent to about 230 K at the height of neutral buoyancy. The region where liquid water can exist is rather limited, extending from about 15 to 30 km in the core of the eruption column. The concentration of water vapor after 30 min is shown in Figure 6. In our scenario, water vapor starts to condense on ash particles at an altitude of about 18 km, at first coating the ash with liquid water. Given the rapid decrease of temperature with height (see Figure 5), however, the high ascent rate of the plume quickly lifts these particles to heights too cold for even supercooled water to exist. Most of the water vapor is thus deposited directly as ice on ash or contributes to the growth of existing ice particles. This occurs both in the core and within the umbrella region, where gravity waves produced by the overshooting lead to upward motion, which in turn produces supersaturation. The eruption clouds of liquid water plus ice after 30 and after 90 min, as well as the

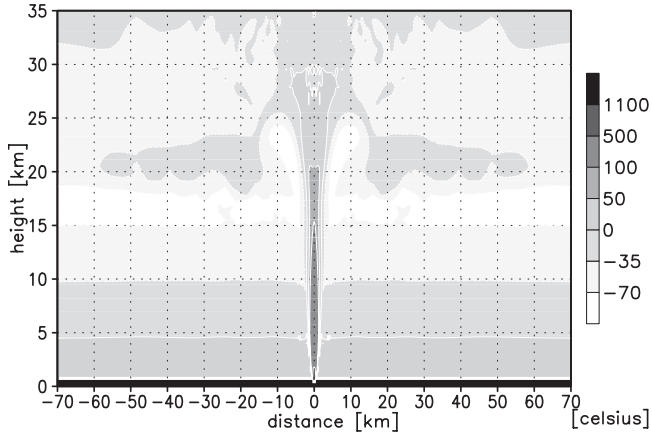

Figure 5. Temperature distribution in degrees Celsius after 30 min, shown for the reference experiment.

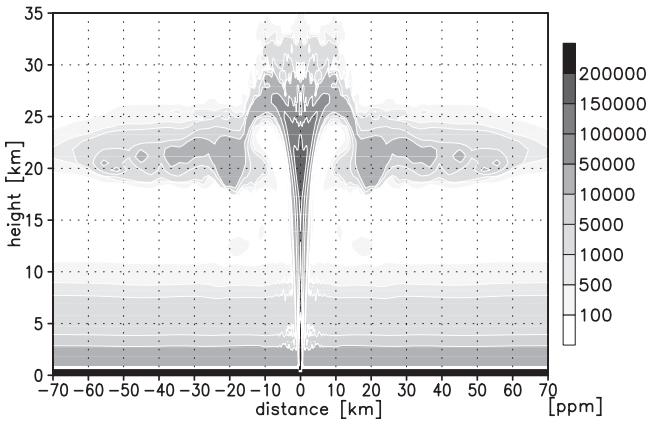

Figure 6. Water vapor concentration in parts per million by volume (ppm), shown for the reference experiment after 30 min.

related vertical distributions of each hydrometeor class are plotted in Figures 7 and 8, respectively.

[48] Liquid water persists only in the core of the plume, with the greater fraction of the hydrometeors in the eruption cloud taking the form of ice particles (>99% by mass after 30 min). This predominance of ice in eruption clouds is supported by observations, as mentioned above in the introduction.

[49] After 30 min, the small 2.5 μm-particle-class represents roughly half of the total ice in the eruption column, see Figure 7. Most of this ice is contained in ash-rich particles, which spread horizontally at the height of neutral buoyancy. Water vapor deposition at cloud top produces relatively ice-rich particles consisting of 20 to 30% ice. During the course of the simulation, the proportion of the larger particle class increases due to aggregation, and by 15 min after the end of the eruption, the mass in the larger class is twice as large as that in the smaller. The larger ice-ash aggregates continue to settle down. The low relative humidity in the lower troposphere in our scenario (see Figure 2), causes sublimation of ice above the melting level. Below an altitude of approximately 8 km, liquid water or ice is entirely evaporated, see Figure 8. Hence no rain reaches the ground. This results in the deposition of completely dry aggregates, although hydrometeors play a significant role during the evolution in the eruption column.

5.2. Scavenging Efficiency and Injection of Volcanic Gases Into the Stratosphere

[50] The concentration of gaseous HCl after 30 min is plotted in Figure 9. The concentration inside the eruption column is 7 to 9 orders of magnitude higher than under background atmospheric conditions. The concentration is slightly reduced in the central plume region between 20 and 25 km, where scavenging by liquid water occurs. The mole fraction of HCl in hydrometeors (not shown) ranges from 0.02 to 0.2 (i.e., from 1 to 10 mol per kg H_2O, or from 3 to 30% by mass). Under the extreme conditions within a volcanic plume (see Figures 5, 6, and 9), condensed phases of crystalline, hydrated HCl, $HCl \cdot 6H_2O$ or even $HCl \cdot 3H_2O$ can theoretically be formed, as discussed in section 3.4. Although the existence of these hydrates affects the solubility of HCl in ice, it would probably not affect the applicability of our parameterization of gas trapping by ice since we employ a purely kinetic approach. The formation of hydrates can also influence the kinetics of deposition of water vapor, which is dependent on its saturation pressure over pure ice in the reference experiment. The specific surface properties of hydrates would be reflected in the mass accommodation coefficient. We did not consider the formation of hydrates, nor the effects of any other solutes. However, given the overall uncertainty of the process under consideration as well as the lack of observations, we believe that such an approximation is justified for the first study of gas incorporation in ice in a volcanic plume.

[51] The shape of the eruption cloud of total HCl (i.e., HCl in all phases) after 30 min, which is shown in Figure 10 looks similar to that of ash (see Figure 3). Most of the erupted HCl has reached the height of neutral buoyancy in the stratosphere. The umbrella region of the HCl plume bears a closer resemblance to the hydrometeor than to the ash plume, in that sedimentation is less pronounced.

[52] Figure 11 shows the vertical distributions of the horizontally integrated mass of HCl per unit height after

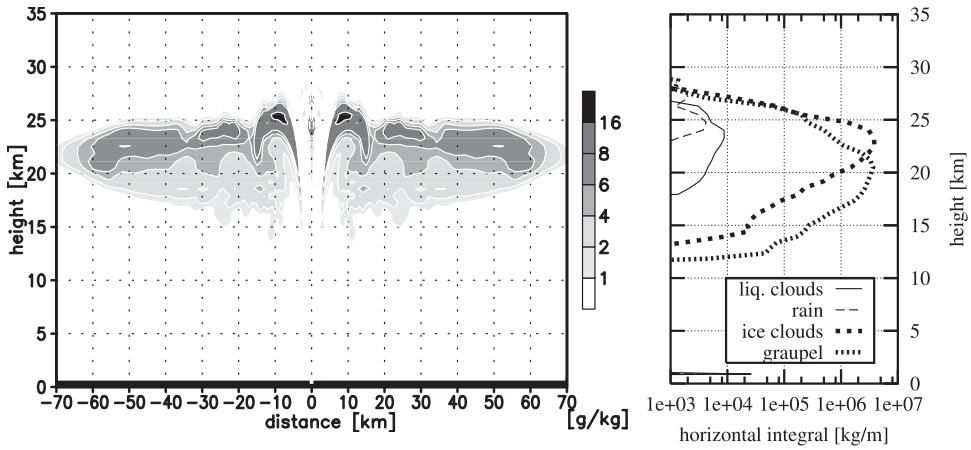

Figure 7. (left) Eruption cloud of all hydrometeors (mass mixing ratio in g/kg). (right) Related vertical distributions of each hydrometeor class (horizontal integral in mass per height level, kg/m). Shown for the reference experiment after 30 min.

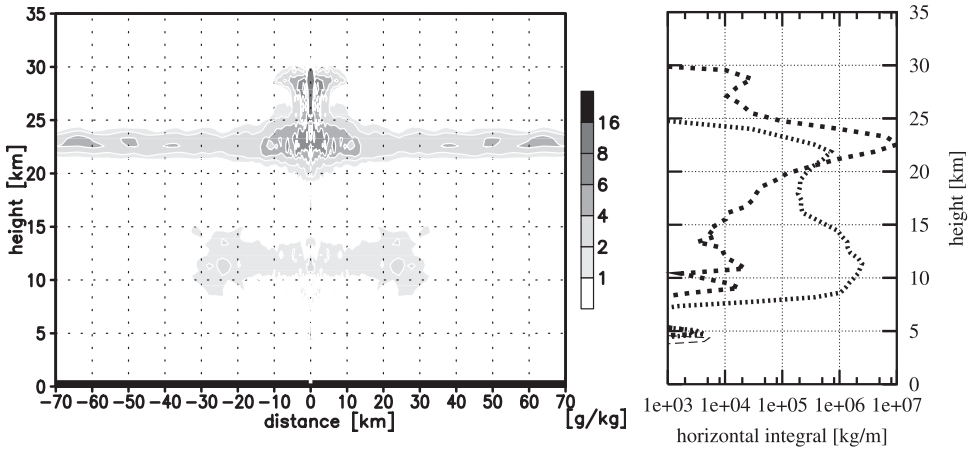

Figure 8. (left) Eruption cloud of all hydrometeors (mass mixing ratio in g/kg). (right) Related vertical distributions of each hydrometeor class (horizontal integral in mass per height level, kg/m). Use key from Figure (7). The horizontal extent of the hydrometeor cloud in the stratosphere is about 250 km. Shown for the reference experiment after 90 min (60 min after the end of the eruption).

30, 60 and 90 min. Despite its high solubility, the fraction of HCl dissolved in water drops is less than 1%. This is because the amount of liquid water in the eruption column is too small to efficiently scavenge HCl. In addition, freezing of drops transfers some HCl to the frozen particle classes. Even one hour after the eruption ends, about half of the HCl can still be found in the gas phase.

[53] At 30 min, about half of the HCl in the eruption column is contained in frozen hydrometeor-ash aggregates, equally distributed between two size classes. HCl contained in the larger aggregates, which arise predominantly from freezing of HCl-bearing drops, precipitates toward lower altitudes. Below 15 km, the amount of HCl in the gas phase increases slightly during the later phase of the eruption (Figure 11). This results from degassing from falling hydrometeors-ash aggregates. Sedimentation transports HCl-containing particles to regions where the gaseous HCl concentration is lower than inside the plume. Complete hydrometeor sublimation below 8 km results in the return of volcanic volatiles to the gas phase. Hence in the fallout of the eruption simulated here no evidence of gas scavenging can be found, although such scavenging plays an important role in the upper parts of the eruption column.

[54] After 30 min, both the shapes of eruption columns of total SO_2 and HCl, as well as the concentration of these gases, are similar (Figures 9 and 10 show the results for HCl.) However, the decrease of the gas concentration in the plume core does not occur for SO_2. The mole fractions of the sulfur gases in hydrometeors are in the order of 10^{-6} to 10^{-3}. The formation of a solid phase like ($SO_2 \cdot 6H_2O$) is possible for gaseous SO_2 concentration greater than about 40.000 ppm [*Huthwelker et al.*, 2001]. As discussed above for HCl, we do not believe that the formation of hydrates would greatly restrict the applicability of our parameterization for gas incorporation.

[55] The vertical distributions of the various phases of SO_2 are depicted in Figure 12. Although the total distributions of HCl and SO_2 are similar, their distribution among phases is not (compare Figures 12 and 11). This is especially evident one hour after the eruption ends. Most of the SO_2 remains in the gaseous phase and spreads horizontally at the height of neutral buoyancy. The scavenging of SO_2 is much less efficient than that of HCl because of its insignificant solubility in water. However, its incorporation into growing ice particles removes about 10% by mass of SO_2 from the gas phase. In Figure 12, there is a distinct peak of SO_2 contained in small frozen particles, which are suspended at 23 km height. Scavenging of SO_2 by larger, falling aggregates, which results in transfer to lower levels, is inefficient, thus tropospheric concentrations are much lower than those for HCl.

[56] The fractions of HCl and SO_2 that reach the stratosphere in relation to the erupted amounts during the course of the simulation are illustrated in Figure 13. These fractions are shown for the species contained in the various hydrometeor classes and in the gas phase, as well as for the total amount occurring in the stratosphere, respectively. We have also included a fictitious, inert tracer in our model eruption. This gas is not scavenged by hydrometeors, but it is passively transported with the mean flow. Its purpose is to estimate the potential volcanic gas injection into the stratosphere. Almost all of this tracer reaches the stratosphere

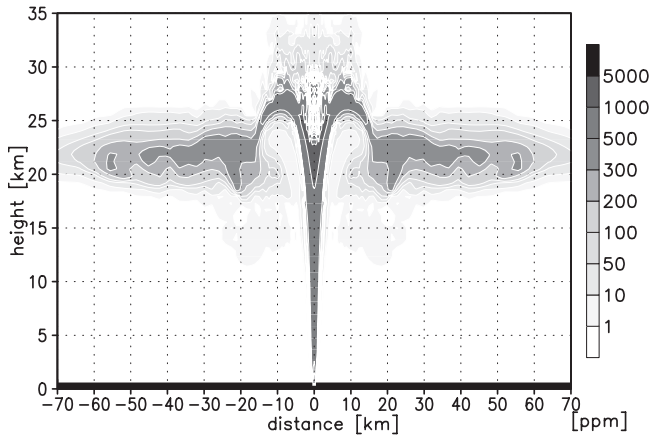

Figure 9. Concentration of gaseous HCl, in parts per million by volume (ppm) shown for the reference experiment after 30 min.

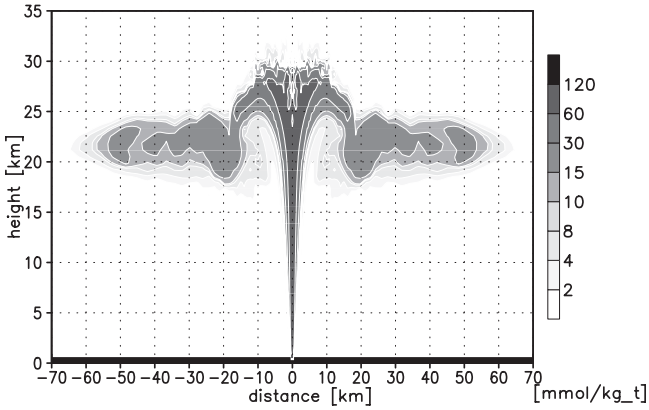

Figure 10. Eruption cloud of total HCl, in mmol/$kg_{totalmass}$, shown for the reference experiment after 30 min.

since the height of neutral buoyancy is well above the tropopause. The collapse of the lower part of the column at the eruption's end produces a rise of the upper part. This results in a posteruptive injection of volcanic gases into the stratosphere, so that >99% of the inert gas can be found in the stratosphere at the end of the simulation. At the same time, most of the ash has already precipitated down to the troposphere as described above. This result of gas-particle separation is supported by satellite observations of the El Chichón plume. Owing to the change of the wind direction with height, the ash particles, which had precipitated to a lower altitude, were transported in an other direction than the gas above. This produced a horizontal separation of particles and gas, which was observed by satellite [*Schneider et al.*, 1999; *Yu and Rose*, 2000].

[57] At the end of the eruption, the fraction of stratospheric HCl is >95%, similar to that of the inert gas. However, only about 60% of this stratospheric HCl is present in the gas phase. The remainder is contained in frozen particles, about 20% each in the small and large size classes. During posteruptive diffusional growth of ice particles in the stratosphere, incorporation of HCl continues until about half of the stratospheric HCl is removed from the gas phase one hour after the eruption ends. Larger particles sediment into the troposphere taking with them the HCl they contain. One hour after the end of the eruption, most of these larger particles are no longer present in the stratosphere, see section 5.1. However, about 70% of the total erupted HCl remains at stratospheric levels.

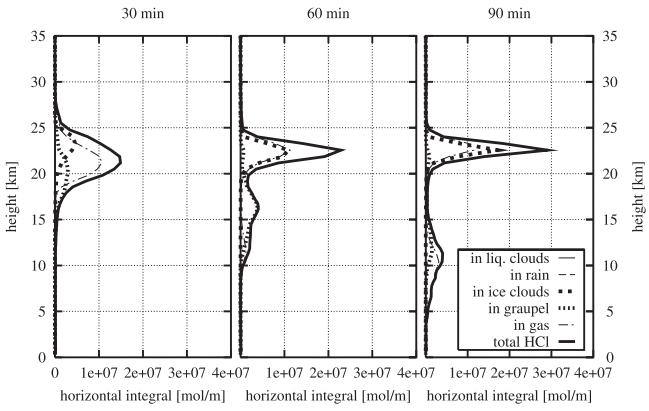

Figure 11. Vertical distributions of HCl in different hydrometeor classes. Horizontal integral in mol/m after 30, 60 and 90 min, shown for the reference experiment.

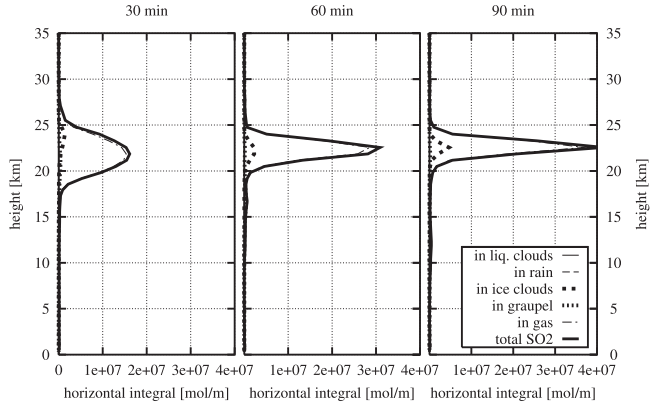

Figure 12. Vertical distributions of SO_2 in different hydrometeor classes. Horizontal integral in mol/m after 30, 60 and 90 min, shown for the reference experiment.

[58] The initial stratospheric fraction of about 99% of the erupted SO_2 is not considerably reduced during or after the eruption because most of this SO_2 is present in the gas phase, and only about 10% is contained in ice. Sedimentation of the larger particles removes about 3%, so that the stratospheric injection of sulfur amounts to about 97% of the erupted amount after 90 min of simulation.

5.3. Effect of Gas Scavenging by Ice

[59] In this section we investigate the influence of gas scavenging by ice particles, for different scavenging efficiencies. Our parameterization of gas incorporation by cocondensation during ice growth is discussed in section 3.2. In the first sensitivity study, called NOINC, the mass accommodation coefficient α_i in equation (4) is set to zero, meaning that we neglect incorporation of volcanic gases into growing ice particles. In the second study, called

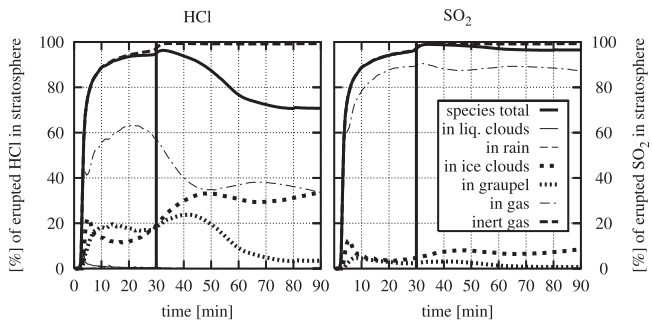

Figure 13. Temporal development of the fractions of (left) HCl and (right) SO_2 in various hydrometeor classes and in the gas phase, that are injected into the stratosphere. "Species total" refers to the stratospheric fraction of the total amount of each of the these gases. For comparison, the stratospheric fraction of an "inert gas" is included, see text. The vertical line at 30 min indicates the end of the eruption. Shown for the reference experiment in percent of total species mass erupted at the vent.

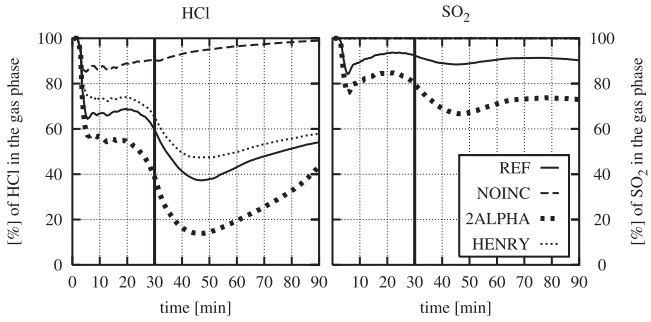

Figure 14. Fractions of (left) HCl and (right) SO_2 in the gas phase as a function of time, in percent by mass. (Fractions of SO_2 for the experiments NOINC and HENRY are so close to 100%, that they are invisible in the plot.) The vertical line at 30 min indicates the end of the eruption. Shown for the sensitivity study on gas trapping in ice.

2ALPHA, the values for α_i are twice as large as in the reference experiment, REF. In the third experiment, dubbed HENRY, we assume that the species concentration in ice particles is limited by the equilibrium concentration in water, which is given by Henry's law. For these experiments, Figure 14 shows the fractions of total HCl and SO_2 present in the gas phase, as a function of time, while Figure 15 shows the corresponding fractions in the stratosphere.

[60] Neglecting gas incorporation into ice, in the experiment NOINC, has a clear effect on the scavenging efficiency for both SO_2 and HCl, as shown in Figure 14. Since SO_2 is practically insoluble in water, it remains completely in the gas phase, and its injection into the stratosphere is similar to that of the inert gas. Also the scavenging efficiency for HCl is strongly diminished in this experiment, despite its high water solubility. HCl scavenging by the smaller ice particle class becomes negligible, and scavenging by the larger class is reduced to half the amount found in the reference experiment, REF. From this we infer that the larger aggregates contained liquid water, which scavenged HCl, during their formation. The presence of water promotes particle growth because the aggregation coefficient of water-covered particles is greater than that of ice-covered particles. The ash-poor, smaller particles, on the other hand, tend to be formed by direct deposition of water vapor on ice.

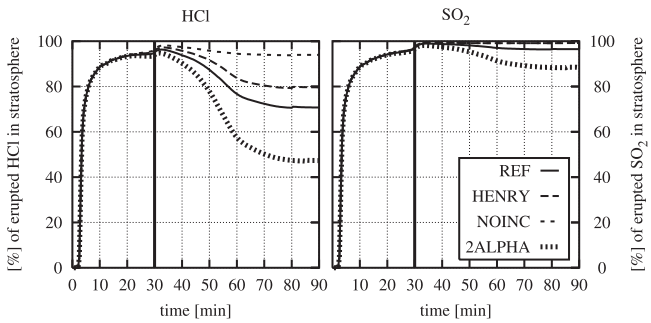

Figure 15. Fractions of (left) HCl and (right) SO_2 in the stratosphere, as a function of time, in percent by mass. The vertical line at 30 min indicates the end of the eruption. Shown for the sensitivity study on gas trapping in ice.

Thus they do not contain HCl if the process of gas trapping by ice is supressed. By the end of our simulation time, HCl in the larger frozen particles has been removed from the stratosphere. About 95% of the HCl can still be found in the stratosphere in the experiment NOINC, (Figure 15), 25% more than in the reference experiment.

[61] Increasing the values for α_i by a factor of two, in the experiment 2ALPHA, increases the scavenging efficiency for SO_2 by more than a factor of two, and decreases the stratosphere SO_2 injection to less than 90% of the erupted SO_2. The removal of SO_2 from the gas phase mainly occurs through scavenging by ice. Doubling α_i for HCl does not affect the gas phase removal as strongly as it does for SO_2, owing to the higher water solubility of the former. The scavenging efficiency for HCl increases by only about 10%. One hour after the eruption ends, the stratospheric injection of HCl is less than 50% of the erupted amount. About 60% of the HCl in the stratosphere is contained in the smaller frozen particle class, which is suspended at the height of neutral buoyancy.

[62] The introduction of the Henry's law limit for the concentration of species in the ice phase, in the experiment HENRY, suppresses the scavenging of SO_2, which remains almost entirely in the gas phase. The scavenging efficiency for HCl is reduced by 10 to 20% and its injection into the stratosphere is increased by the same amount when compared to the reference experiment. At the end of the experiment HENRY, about 80% of the HCl remains in the stratosphere.

[63] Our sensitivity studies suggest that the incorporation of gases into growing ice particles has a significant impact on the scavenging efficiency for volcanic gases and their injection into the stratosphere, and further that gas incorporation into ice particles is highly sensitive to the value of the mass accommodation coefficient. These results await experimental verification; to our knowledge there are no observational data for gas scavenging by ice particles in volcanic eruption clouds. This situation should be improved in order to better estimate the climatic impact of volcanic eruptions.

5.4. Impact of the Salinity Effect

[64] In this section we consider the effects of dissolved volcanic gases on the thermodynamic properties of water

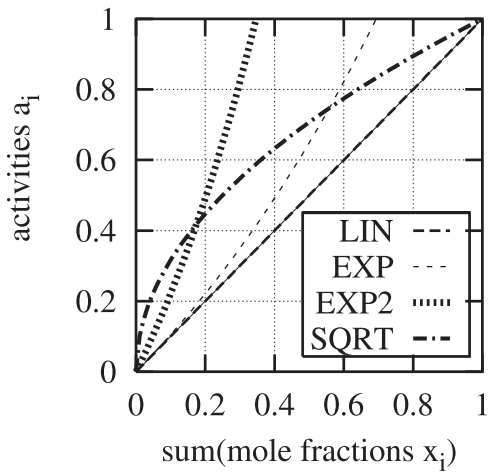

Figure 16. Salinity effect: functions for activity.

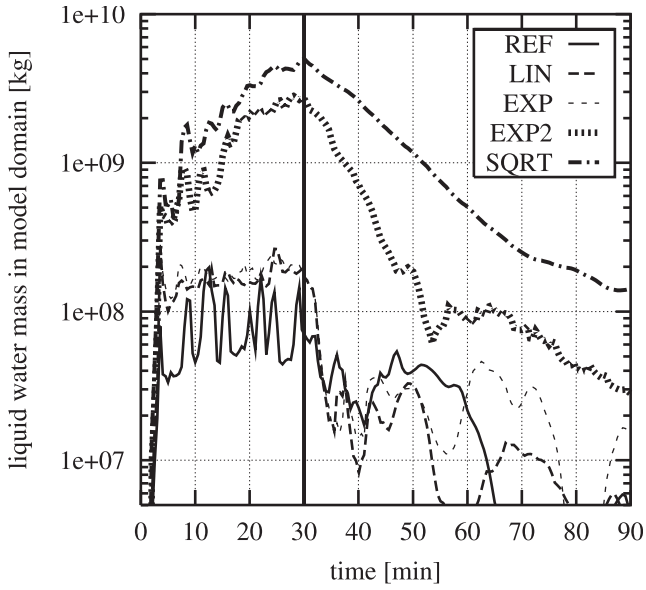

Figure 17. Total mass of liquid water in the model domain in kg, shown for the sensitivity study on the salinity effect. The vertical line at 30 min indicates the end of the eruption.

and ice (see section 3.4) We investigate the feedback of salinity effects on the scavenging efficiency for volcanic gases, and on their injection into the stratosphere. We employ equations (7) and (8) for vapor pressure and freezing temperature depression, respectively. To account for the nonideal solute effects, we replace the mole fractions x_i by the various expressions for the activities, a_i, as shown in equation (9) and Figure 16. This last step is undertaken in order to simulate a range of more realistic solutions.

$$\begin{aligned}
\text{REF}: &\quad a_{ref}\left(\sum_{i=1}^{n} x_i\right) &&= 0. \\
\text{LIN}: &\quad a_{lin}\left(\sum_{i=1}^{n} x_i\right) &&= \sum_{i=1}^{n} x_i \\
\text{EXP}: &\quad a_{exp}\left(\sum_{i=1}^{n} x_i\right) &&= exp\left(\sum_{i=1}^{n} x_i\right) - 1 \\
\text{EXP2}: &\quad a_{exp2}\left(\sum_{i=1}^{n} x_i\right) &&= exp\left(2 * \sum_{i=1}^{n} x_i\right) - 1 \\
\text{SQRT}: &\quad a_{sqrt}\left(\sum_{i=1}^{n} x_i\right) &&= sqrt\left(\sum_{i=1}^{n} x_i\right)
\end{aligned} \tag{9}$$

[65] In the reference experiment, REF, we neglect the solute effects. In the experiment LIN, the hydrometeors are treated like ideal solutions. In the experiment EXP we assume an exponential dependence of the salinity effect on the mole fraction; in the experiment EXP2 this feature is enhanced by multiplying the mole fraction in the exponent by a factor of two. The function applied in the experiment SQRT exaggerates the effect of low solute concentration, it serves as an upper-limit estimation of the salinity effect for low solute concentrations. As mentioned in section 5.2, the mole fraction of HCl in hydrometeors in the reference experiment ranges from 0.02 to 0.2. Hence the salinity effect in our experiments increases in the following sequence: LIN < EXP < EXP2 < SQRT. The freezing point depression resulting from these activities is in the range of those shown in the work of *Thibert and Dominé* [1997], and it covers the uncertainty range of possible values. In all likelihood, our parameterizations do not correspond to the real activities. However, these experiments are still useful for gaining a better idea of the importance of the salinity effect in volcanic eruption columns, given the lack of knowledge concerning the composition and solute concentration in hydrometeors in a volcanic eruption column.

[66] We assume in our simulations that the depression of the freezing point is limited by the eutectic temperature of HCl solutions, $T_{f,min}$ = 198.45 *K* [*Thibert and Dominé*, 1997] because HCl is the solute with the highest concentration in the drops. According to equation (8), the maximum activity allowed in all experiments is thus a = 0.72.

[67] Considering all the salinity effect experiments, the total mass of liquid water plus ice increases by no more than 10%, compared with the reference experiment, REF. The total mass of liquid water is shown in Figure 17. In the experiments LIN and EXP, it is not much different than in REF, while it is greater by more than a factor of 10 for the experiments EXP2 and SQRT. However, even in the latter two experiments, about 90% of the total hydrometeor mass exists in the form of ice.

[68] Owing to the increased availability of liquid water, the scavenging efficiency for HCl, which is highly water soluble, is increased. The fraction of HCl remaining in the gas phase during the 30 min of eruption is reduced from about 60% in the experiment REF to about 20 and 10% in the experiments EXP2 and SQRT, respectively. However, the amount of volcanic gases in the stratosphere remains similar since HCl contained in hydrometeors reaches the same height as that in the gas phase. It is only after the eruption ends, that of portion of the HCl-bearing particles is removed from the stratosphere by sedimentation. The fractions of erupted HCl and SO_2 that can be found in the stratosphere during the course of the various experiments are shown in Figure 18. One hour after the eruption has ended, about 30% of the HCl remains in the stratosphere, for the experiments EXP2 and SQRT.

[69] In experiment SQRT, the mass fraction of frozen particles in the larger class is greater than in to the other experiments. This is an effect of increased aggregation

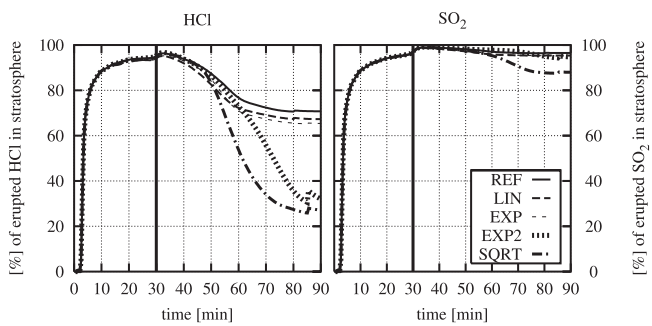

Figure 18. Fractions of total (left) HCl and (right) SO_2 present in the stratosphere, as a function of time, in percent by mass. The vertical line at 30 min indicates the end of the eruption. Shown for the sensitivity study on the salinity effect.

efficiency, due, in turn, to the increase of liquid water. Hence SO_2 contained in these particles is removed from the stratosphere by sedimentation and the stratospheric SO_2 injection at the end of our simulation time is reduced to about 90% of the erupted amount.

6. Discussion

[70] Using the ATHAM model, we have performed numerical simulations of an idealized Plinian volcanic eruption under subtropical atmospheric conditions. We investigated the scavenging of volcanic gases in the rising plume and their injection into the stratosphere. The ATHAM model includes all the dynamical, microphysical, and physicochemical processes believed to be important in volcanic eruption columns. We have used simple parameterizations of gas scavenging in order to identify the important processes controlling the scavenging efficiency and the parameters which determine these processes. Gas trapping in ice particles has been shown to be relevant, but our parameterization of gas incorporation awaits laboratory and possibly field verification.

[71] The results presented here were obtained from simulations utilizing a single volcanic forcing, and for a single set of environmental conditions. Each individual volcanic eruption, however, behaves very specifically, depending on the volcanic forcing (magma composition and temperature, gas content, vertical velocity) and on the ambient atmospheric conditions (stability, humidity, wind); for an overview, see, e.g., *Sparks et al.*, [1997]. The scavenging efficiency for volcanic gases may be affected by the these factors since it depends on the amount of condensed water in the plume. An eruption with a higher availability of water or ice will have an increased overall scavenging efficiency and will thus result in reduced stratospheric gas injection. Water in the plume may derive from the magma itself, or may result from interaction of magma with surface or subsurface water in so-called phreatomagmatic eruptions, or from entrainment of moist air from an ambient atmosphere with a high specific humidity. The ratio of liquid water to ice in the plume, which influences in particular the scavenging of soluble gases like HCl, is determined by the temperature distribution in the eruption column. We performed sensitivity studies (not shown here) for different environmental and volcanic conditions, e.g., various particles size distributions. We found that although the ratios for the scavenging efficiency and the gas injection into the stratosphere change slightly, the principal findings of this study are still valid. We would only expect significant deviations in the case of eruptions containing very large amounts of water or ice in the eruption column, such as phreatomagmatic events.

[72] Volcanoes are thought to inject about 10 to 100 times more H_2O (vapor and ice) than sulfur into the stratosphere [*Tabazadeh and Turco*, 1993]. The exact amount of H_2O has not yet been quantified, but our simulations suggest that it is considerable. The numerical simulations of *Glaze et al.*, [1997] with a one dimensional model indicate that large volcanic eruptions can deposit a mass of water in the stratosphere equivalent to up to 7% of total stratospheric water burden, and our simulations confirm these results. An increased stratospheric concentration of H_2O may accelerate SO_2 and H_2S oxidation, and may also influence the composition of sulfate aerosol, and hence the radiative forcing ultimately produced by the eruption. Our findings suggest that the posteruptive increase of stratospheric SO_2 observed by satellites is due to both the sublimation of sulfur-containing ice and H_2S oxidation. The oxidation of H_2S in the stratosphere produces additional H_2O, which in turn influences stratospheric dynamics, microphysics and chemistry. These posteruptive processes are not considered in the framework of our research, but they must be taken into account when considering the climatic impact of explosive volcanic eruptions.

[73] This study confirms the results of *Tabazadeh and Turco* [1993] (T&T93) in that a high fraction of SO_2 reaches the stratosphere, while a much lower fraction is indicated for HCl. The top-hat geometry and the steady state assumption in the plume model of *Woods* [1988] used by T&T93 enabled a relatively simple formulation of the dynamics. In addition, the microphysics was strongly simplified, precipitation of hydrometeors or ash aggregation was not considered, sedimentation and re-entrainment of tracers were all neglected. Further, condensation of water was assumed to take place on sulfate aerosol particles emitted by the volcano, but not on volcanic ash. Since such sulfate particles are smaller than the critical radius for a stable particle, condensation of water is delayed in the T&T93 model. In ATHAM, since the abundant, relatively large volcanic ash particles act as cloud condensation nuclei, supersaturation due to surface tension effects is not to be expected. T&T93 assumed that the existence of supercooled drops was favored over ice formation. They employed the phase diagram of the HCl/H_2O system to show that concentrated HCl-H_2O drops can still exist at temperatures well below the freezing temperature of pure supercooled water. We have investigated the freezing point depression in the sensitivity studies considering the salinity effect, and we still find a high predominance of frozen hydrometeors. This difference is probably caused by the top-hat geometry of the plume model of *Woods* [1988], which predicts a higher temperature in the eruption column than the ATHAM model used in this study. The Woods model did not include the ice phase. Instead, all hydrometeors were assumed to be supercooled water drops or aqueous solutions. Gas trapping in ice was not considered. T&T93 parameterized the scavenging of chemical species in the eruption column by assuming solubility equilibrium in supercooled drops. Consequently the scavenging efficiency for SO_2 was very small and it all reached the stratosphere. In our study, the sulfur gases are partly scavenged by growing ice particles. The high scavenging efficiency and the negligible injection into the stratosphere for HCl found by T&T93 is a consequence of the greater water availability in their plume model. Our study, which employed a more comprehensive representation of the dynamics and the microphysics, shows considerable input of HCl into the stratosphere. Thus we believe that ozone destruction caused by direct HCl injection into the stratosphere during highly explosive volcanic eruptions cannot be completely ruled out.

7. Conclusions

[74] We have examined the scavenging of the most important volcanic gases, HCl, SO_2 and H_2S, by liquid

and solid hydrometeors and by aggregates, in a Plinian eruption column. The aggregates contain very little water or ice, and the ash fraction was in general higher than 80% in our simulations. The greatest fraction of hydrometeors exists as ice because the temperature is below −35°C in most parts of the eruption cloud. The salinity effect increases the amount of liquid water by up to a factor of ten, but frozen hydrometeors still predominant strongly. We used simplifying parameterizations to estimate the effect of solutes on the thermodynamic quantities of the hydrometeors since at present no observations from inside volcanic eruption columns are available. Observations, although technically challenging, are urgently needed.

[75] As a consequence of the lack of liquid water, the scavenging efficiency for HCl was much lower than might have been expected from its high water solubility, and only 1% of total HCl was found in liquid water. However, scavenging of HCl by ice particles via direct gas incorporation during diffusional ice growth was found to be of considerable importance. The salinity effect increases the total scavenging efficiency from about 50% to about 90%.

[76] The sulfur-containing gases SO_2 and H_2S are only slightly soluble, hence their scavenging by liquid water is negligible. However, these gases are incorporated into growing ice particles with a scavenging efficiency of 10 to 30% by mass. Ignoring this effect might well lead to an overestimation of volcanic sulfur injection into the stratosphere. The efficiency of gas trapping in ice is highly sensitive to the mass accommodation coefficients. There is thus a strong need for better determination of these coefficients in the laboratory.

[77] Despite scavenging, more than 25% of the HCl and 80% of the sulfur gases erupted at the vent can be found in the stratosphere, one hour after the eruption ends. This is because the most of the particles containing these species reached in the stratosphere. Hence we find a considerable direct HCl injection into the stratosphere, suggesting the possibility of ozone destruction by chlorine of volcanic origin. Plinian eruptions might have had a detrimental effect on stratospheric ozone well before the increase of anthropogenic chlorine.

[78] **Acknowledgments.** This research was supported by the Volkswagen Foundation under the Emission of Volcanic Volatiles Into the Atmosphere (EVA) project. Reviews by two anonymous reviewers and Arthur Greene have significantly improved the text.

References

Angell, J. L., Estimated impact of Agung, El Chichón and Pinatubo volcanic eruptions on global and regional total ozone after adjustment for the QBO, *Geophys. Res. Lett.*, *24*(6), 647–650, 1997.

Atkins, P. W., *Physical Chemistry*, Oxford Univ. Press, New York, 1986.

Bacon, C. R., S. Newman, and E. Stolper, Water, CO_2, Cl, and F in melt inclusions in phenocrysts from 3 holocene explosive eruptions, Crater Lake, Oregon, *Am. Mineral.*, *77*(9–10), 1021–1030, 1992.

Banham, S. F., J. R. Sodea, A. B. Horn, M. R. S. McCoustra, and M. A. Chesters, Adsorption and ionization of HCl on an ice surface, *J. Vac. Sci. Technol. A*, *14*(3), 1620–1626, 1996.

Bluth, G. J. S., S. D. Doiron, C. C. Schnetzler, A. J. Krueger, and L. S. Walter, Global tracking of the SO_2 cloud from the June, 1991 Mount Pinatubo eruptions, *Geophys. Res. Lett.*, *19*(2), 151–154, 1992.

Bluth, G. J. S., C. J. Scott, I. E. Sprod, C. C. Schnetzler, A. J. Krueger, and L. S. Walter, Explosive SO_2 emissions from the 1992 eruptions of Mount Spurr, Alaska, *U.S. Geol. Surv. Bull.*, *2139*, 37–45, 1995.

Brasseur, G. P., C. Granier, and S. Walters, Future changes in stratospheric ozone and the role of heterogeneous chemistry, *Nature*, *348*, 626–628, 1990.

Bureau, H., H. Keppler, and N. Métrich, Volcanic degassing of bromine and iodine: Experimental fluid/melt partitioning data and applications to stratospheric chemistry, *Earth Planet. Sci. Lett.*, *183*, 51–60, 2000.

Carey, S., and H. Sigurdsson, Influence from particle aggregation on deposition of distal tephra from the May 18, 1980, eruption of Mount St. Helens volcano, *J. Geophys. Res.*, *87*(B8), 7061–7072, 1982.

Carslaw, K. S., T. Peter, and S. L. Clegg, Modeling the composition of liquid stratospheric aerosols, *Rev. Geophys.*, *35*(2), 125–154, 1997.

Chen, J.-P., and P. J. Crutzen, Solute effect on the evaporation of ice particles, *J. Geophys. Res.*, *99*(D9), 18,847–18,859, 1994.

Clapsaddle, C., and D. Lamb, The sorption behavior of SO_2 on ice at temperatures between −30°C and −50°C, *Geophys. Res. Lett.*, *16*(10), 1173–1176, 1989.

Conklin, M. H., and R. C. Bales, SO_2 uptake on ice spheres: Liquid nature of the ice-air interface, *J. Geophys. Res.*, *98*, 16,851–16,855, 1993.

Conklin, M. H., R. A. Sommerfeld, S. K. Layrd, and J. E. Vilinski, Sulfur dioxide reaction on ice surfaces: Implications for dry deposition to snow, *Atmos. Environ. Part A*, *27*, 159–166, 1993.

Delmas, R. J., Antarctic precipitation chemistry, in *Chemistry of Multiphase Atmospheric Systems*, *NATO ASI Ser.*, vol. G6, edited by W. Jaeschke, pp. 249–266, Springer-Verlag, New York, 1986.

DeMore, W. B., S. P. Sander, D. M. Golden, R. F. Hampson, M. J. Kurylo, D. J. Howard, A. R. Ravishankara, C. E. Kolb, and M. J. Molina, Chemical kinetics and photochemical data for use in stratospheric modeling, *JPL Publ. 92-20*, Jet Propulsion Lab., Pasadena, Calif., 1997.

Diehl, K., S. K. Mitra, and H. R. Pruppacher, A laboratory study on the uptake of HNO_3 and HCl vapor by snow crystals and ice spheres at temperatures between 0 and −40°C, *Atmos. Environ.*, *29*(9), 975–981, 1995.

Diehl, K., S. K. Mitra, and H. R. Pruppacher, A laboratory study on the uptake of HCl, HNO_3 and SO_2 gas by ice crystals and the effect of these gases on the evaporation rate of the crystals, *Atmos. Res.*, *47/48*, 235–244, 1998.

Dominé, F., and E. Thibert, Mechanisms of incorporation of trace gases in ice grown from the gas phase, *Geophys. Res. Lett.*, *23*, 3627–3630, 1996.

Dominé, F., and I. Xueref, Evaluation of depth profiling using laser resonant desorption as a method to measure diffusion coefficients in ice, *Anal. Chem.*, *73*, 4348–4353, 2001.

Dominé, F., E. Thibert, E. Silvente, M. Legrand, and J. Jaffrezo, Determining past atmospheric HCl mixing ratios from ice core analysis, *J. Atmos. Chem.*, *21*, 165–186, 1995.

Ernst, G. G. J., J. P. Davis, and R. S. J. Sparks, Bifurcation of volcanic plumes in a crosswind, *Bull. Volcanol.*, *57*, 159–169, 1994.

Faraday, M., On regulation, and on observation of force, *Philos. Mag.*, *17*, 162–169, 1859.

Gerlach, T. M., and T. Casadevall, Fumarole emissions at Mount St. Helens Volcano, June 1980 to October 1981: Degassing of a magma-hydrothermal system, *J. Volcanol. Geotherm. Res.*, *28*, 141–160, 1986.

Gerlach, T. M., H. R. Westrich, and R. B. Symonds, Preeruption vapor in magma of the climactic Mount Pinatubo eruption: Source of the giant stratospheric sulfur dioxide cloud, in *Fire and Mud: Eruptions and Lahars of Mount Pinatubo*, edited by C. G. Newhall and R. S. Punongbayan, pp. 415–433, Philippine Inst. of Volcanol. and Seismol., Univ. of Wash. Press, Seattle, Wash., 1996.

Glaze, L. S., S. M. Baloga, and L. Wilson, Transport of atmospheric water vapor by volcanic eruption columns, *J. Geophys. Res.*, *102*(D5), 6099–6108, 1997.

Graf, H.-F., M. Herzog, J. M. Oberhuber, and C. Textor, The effect of environmental conditions on volcanic plume rise, *J. Geophys. Res.*, *104*, 24,309–24,320, 1999.

Granier, C., and G. Brasseur, Impact of heterogeneous chemistry on model predictions of ozone changes, *J. Geophys. Res.*, *97*, 18,015–18,033, 1992.

Haynes, D. R., N. J. Tro, and S. M. George, Condensation and evaporation of H_2O on ice surfaces, *J. Phys. Chem.*, *9*(21), 8502–8509, 1992.

Herzog, M., Simulation der Dynamik eines Multikomponentensystems am Beispiel vulkanischer Eruptionswolken, Ph.D. thesis, Univ. of Hamburg, Hamburg, 1998.

Herzog, M., H.-F. Graf, C. Textor, and J. M. Oberhuber, The effect of phase changes of water on the development of volcanic plumes, *J. Volcanol. Geotherm. Res.*, *87*, 55–74, 1998.

Herzog, M., J. M. Oberhuber, and H.-F. Graf, A prognostic turbulence scheme for the non-hydrostatic plume model ATHAM, *J. Atmos. Sci*, in press, 2003.

Hofmann, D. J., and S. Solomon, Ozone destruction through heterogeneous chemistry following the eruption of El Chichón, *J. Geophys. Res.*, *94*, 5029–5041, 1989.

Holdsworth, G., H. R. Krouse, and E. Peake, Relationship between volcanic emission peaks and the oxygen isotope signature in an ice core from the Yukon territory, Canada, *Eos Trans. AGU*, *67*, 883, 1986.

Huthwelker, T., D. Lamb, M. Baker, B. Swanson, and T. Peter, Uptake of SO_2 by polycrystalline water ice, *J. Colloid. Interf. Sci.*, *238*(1), 147–159, 2001.

Iribarne, J. V., and T. Pyshnov, The effect of freezing on the compositions of supercooled droplets - I. Retention of HCl, NH_3, and H_2O_2, *Atmos. Environ. Part A*, *24*(2), 383–387, 1990.

Iribarne, J. V., L. A. Barrie, and A. Iribarne, Effect of freezing on sulfur dioxide dissolved in supercooled droplets, *Atmos. Environ.*, *17*(5), 1047–1050, 1983.

Iribarne, J. V., T. Pyshnov, and B. Naik, The effect of freezing on the compositions of supercooled droplets - II. Retention of S(IV), *Atmos. Environ. Part A*, *24*(2), 389–398, 1990.

Kim, Y. P., and J. H. Seinfeld, Atmospheric gas-aerosol equilibrium. I: Thermodynamic model, atmospheric gas-aerosol equilibrium, *Aerosol Sci. Technol.*, *19*, 157–181, 1993a.

Kim, Y. P., and J. H. Seinfeld, Atmospheric gas-aerosol equilibrium. II: Analysis of common approximations and activity calculation methods, *Aerosol Sci. Technol.*, *19*, 182–198, 1993b.

Kotra, J. P., D. L. Finnegan, W. H. Zoller, M. A. Hart, and J. L. Moyers, El Chichn: Composition of plume gases and particles, *Science*, *222*, 1018, 1983.

Krotkov, N. A., and A. J. Krueger, Composition of the plume from the February 26, 2000 eruption of Mt. Hekla, Iceland: A combined satellite-model study, *Eos Trans. AGU*, *81*(48), Fall Meet. Suppl., Abstract V61B-10, 2000.

Krueger, A. J., L. S. Walter, P. K. Bhartia, C. C. Schnetzler, N. A. Krotkov, I. Sprod, and G. J. S. Bluth, Volcanic sulfur dioxide measurements from the total ozone mapping spectrometer instruments, *J. Geophys. Res.*, *100*, 14,057–14,076, 1995.

Laj, P., et al., Behaviour of H_2O_2, NH_3, and black carbon in mixed-phase clouds during CIME, *Atmos. Res.*, *58*, 315–336, 2001.

Lamb, D., and R. Blumenstein, Measurements of an entrapment of sulfur dioxide by rimed ice, *Atmos. Res.*, *21*, 1765–1772, 1987.

Levine, I. N., *Physical Chemistry*, 4th ed., Mc Graw-Hill, New York, 1995.

Luhr, J. F., I. S. E. Carmichael, and J. C. Varekamp, The 1982 eruptions of El Chichón volcano, Chiapas, Mexico: Mineralogy and petrology of the anhydrite-bearing pumices, *J. Volcanol. Geotherm. Res.*, *23*, 69–108, 1984.

Mackinnon, I. D. R., J. L. Gooding, D. S. McKay, and U. S. Clanton, The El Chichón stratospheric cloud: Solid particulates and settling rates, *J. Volcanol. Geotherm. Res.*, *23*, 125–146, 1984.

Mankin, W. G., and M. T. Coffey, Increased stratospheric hydrogen chloride in the El Chichón cloud, *Science*, *226*, 170–172, 1984.

Mankin, W. G., M. T. Coffey, and A. Goldman, Airborne observations of SO_2, HCl, and O_3 in the stratospheric plume of the Pinatubo Volcano in July 1991, *Geophys. Res. Lett.*, *19*(2), 179–182, 1992.

Mari, C., D. J. Jacob, and P. Bechthold, Transport and scavenging of soluble gases in a deep convective cloud, *J. Geophys. Res.*, *105*(D7), 22,255–22,267, 2000.

Mayberry, G. C., W. I. Rose, and G. J. S. Bluth, Dynamics of the volcanic and meteorological clouds produced by the December 26, 1997 eruption of Soufrire Hills Volcano, Montserrat, W.I., in *The Eruption of Soufrire Hills Volcano, Montserrat, 1995-99*, vol. 21, edited by T. Druitt and P. Kokelaar, pp. 539–555, Geol. Soc. of London, 2001.

McClatchey, R. A., R. W. Fenn, J. E. A. Selby, F. E. Volz, and J. S. Garing, Optical properties of the atmosphere, *Environ. Res. Pap.*, *411*, 1972.

McCormick, M. P., L. W. Thomason, and C. R. Trepte, Atmospheric effects of the Mt. Pinatubo eruption, *Nature*, *373*(2), 399–404, 1995.

McKeen, S. A., S. C. Liu, and C. S. Kiang, On the chemistry of stratospheric SO_2 from volcanic eruptions, *J. Geophys. Res.*, *89*(D3), 4873–4881, 1984.

Meyers, M. P., R. L. Walko, J. Y. Harrington, and W. R. Cotton, New RAMS cloud microphysics parameterization. part II: The two moment scheme, *Atmos. Res.*, *45*, 3–39, 1997.

Mitra, S. K., S. Barth, and H. R. Pruppacher, A laboratory study on the scavenging of SO_2 by snow crystals, *Atmos. Environ. Part A*, *24*(9), 2307–2312, 1990.

Oberhuber, J. M., M. Herzog, H.-F. Graf, and K. Schwanke, Volcanic plume simulation on large scales, *J. Volcanol. Geotherm. Res.*, *87*, 29–53, 1998.

Press, W. H., S. A. Teukolsky, W. T. Vetterling, and B. P. Flannery, *Numerical Recipes in FORTRAN, The Art of Scientific Computing*, 2nd ed., Cambridge Univ. Press, New York, 1992.

Pruppacher, H. R., and J. D. Klett, *Microphysics of Clouds and Precipitation*, 2nd ed., Kluwer Acad., New York, 1997.

Rose, W. I., D. Delene, D. Schneider, G. Bluth, A. Krueger, I. Sprod, C. McKee, H. Davies, and G. G. J. Ernst, Ice in the 1994 Rabaul eruption cloud: Implications for volcano hazard and atmospheric effects, *Nature*, *375*, 477–479, 1995.

Rose, W. I., G. J. S. Bluth, and G. G. J. Ernst, Integrating retrievals of volcanic cloud characteristics from satellite remote sensors: A summary, *Philos. Trans. R. Soc. A*, *358*, 1538–1606, 2000.

Rose, W. I., G. J. S. Bluth, D. J. Schneider, G. G. J. Ernst, C. M. Riley, L. J. Henderson, and R. G. McGimsey, Observations of volcanic clouds in their first few days of atmospheric residence: The 1992 eruptions of Crater Peak, Mount Spurr volcano, Alaska, *J. Geol.*, *6*, 677–694, 2001.

Rye, R. O., J. F. Luhr, and M. D. Wasserman, Sulfur and oxygen isotopic systematic of the 1982 eruptions of El Chichón volcano, Mexico, *J. Volcanol. Geotherm. Res.*, *23*, 109–122, 1984.

Sachs, P. M., and E. Harms, Atmospheric release of Br, I, Cl, F and SO_2 by the Laacher See volcanic eruption (Germany), 12000 BP, oral presentation at the 78. Jahrestagung der Deutschen Mineralogischen Gesellschaft (DMG) Symposium 9: Fluids, Melts, and Mineralisation, 24–29 Sept. 2000, Heidelberg, 2000.

Sander, R., Modeling atmospheric chemistry: Interactions between gas-phase species and liquid cloud/aerosol particles, *Surv. Geophys.*, *20*(1), 1–31, 1999.

Santachiara, G., F. Prodi, and F. Vivarelli, Scavenging of SO_2 and HCl during growth of ice crystals by vapour diffusion, *Atmos. Environ.*, *29*(9), 983–987, 1995.

Santachiara, G., F. Prodi, R. Udisti, and A. Prodi, Scavenging of SO_2 and NH_3 during growth of ice, *Atmos. Res.*, *47–48*(9), 209–217, 1998.

Schneider, D. J., and W. I. Rose, Observations of the 1989–90 Redoubt Volcano eruption clouds using AVHRR satellite imagery, in *Proceedings of International Symposium on Volcanic Ash and Aviation Safety*, vol. 2047, edited by T. Casadevall, pp. 405–418, U.S. Geol. Surv. Bull., 1994.

Schneider, D. J., W. I. Rose, L. R. Coke, and G. J. S. Bluth, Early evolution of a stratospheric volcanic eruption cloud as observed with TOMS and AVHRR, *J. Geophys. Res.*, *104*(D4), 4037–4050, 1999.

Schwartz, S. E., Mass-transport consideration pertinent to aqueous phase reactions of gases in liquid water clouds, in *Chemistry of Multiphase Atmospheric Systems*, *NATO ASI Ser.*, vol. G6, edited by W. Jaeschke, pp. 415–471, Springer-Verlag, New York, 1986.

Simkin, T., Terrestrial volcanism in space and time, *Ann. Rev. Earth Planet. Sci.*, *21*, 427–452, 1993.

Smith, B. D., R. A. Zielinski, W. I. Rose, and B. J. Huebert, Water-soluble material on aerosols collected within volcanic eruption clouds, *J. Geophys. Res.*, *87*(C7), 4963–4972, 1982.

Solomon, S., R. W. Sanders, R. R. Garcia, and J. G. Keys, Increased stratospheric chlorine dioxide over Antarctica caused by volcanic aerosols from Mount Pinatubo, *Nature*, *336*, 245–248, 1993.

Solomon, S., R. W. Portmann, R. R. Garcia, L. W. Thomason, L. R. Poole, and M. P. McCormick, The role of aerosol variations in anthropogenic ozone depletion at northern midlatitudes, *J. Geophys. Res.*, *101*, 6713–6727, 1996.

Solomon, S., R. W. Portmann, R. R. Garcia, W. Randel, F. Wu, R. Nagatani, J. Gleason, L. W. Thomason, L. R. Poole, and M. P. McCormick, Ozone depletion at midlatitudes: Coupling of volcanic aerosols and temperature variability to anthropogenic chlorine, *Geophys. Res. Lett.*, *25*(11), 1871–1874, 1998.

Sommerfeld, R. A., and D. Lamb, Preliminary measurements of SO_2 adsorbed on ice, *Geophys. Res. Lett.*, *13*(4), 349–351, 1986.

Sparks, R. S. J., M. I. Bursik, S. N. Carey, J. S. Gilbert, L. Glaze, H. Sigurdsson, and A. W. Woods, *Volcanic Plumes*, John Wiley, Hoboken, N. J., 1997.

Symonds, R. B., W. I. Rose, and M. H. Reed, Contribution of Cl- and F-bearing gases to the atmosphere by volcanoes, *Nature*, *334*, 415–418, 1988.

Symonds, R. B., W. I. Rose, G. J. S. Bluth, and T. M. Gerlach, Volcanic gas studies: Methods, results and applications, in *Volatiles in Magma*, *Rev. Mineral.*, vol. 30, edited by M. R. Carrol and J. R. Holloway, pp. 1–66, Mineral Soc. of Am., 1994.

Tabazadeh, A., and R. P. Turco, Stratospheric chlorine injection by volcanic eruptions: HCl scavenging and implications for ozone, *Science*, *260*, 1082–1086, 1993.

Textor, C., Numerical simulation of scavenging processes in explosive volcanic eruption clouds, Ph.D. thesis, Univ. of Hamburg, Hamburg, 1999.

Textor, C., P. M. Sachs, H.-F. Graf, and T. H. Hansteen, The 12,900 yr BP Laacher See eruption: Estimation of volatile yields and simulation of their fate in the plume, in *Volcanic Degassing*, edited by D. P. C. Oppenheimer and J. Barclay, Geol. Soc., London, in press, 2003.

Thibert, E., and F. Dominé, Thermodynamics and kinetics of the solid solution of HCl in ice, *J. Phys. Chem. B*, *101*, 3554–3565, 1997.

Tie, X. X., and G. Brasseur, The response of stratospheric ozone to volcanic eruptions - sensitivity to atmospheric chlorine loading, *Geophys. Res. Lett.*, *22*(22), 3035–3038, 1995.

Toohey, D. W., L. M. Avallone, L. R. Lait, P. A. Neuman, M. R. Schoeberl, D. W. Fahey, E. L. Woodbridge, and J. G. Anderson, The seasonal evolution of reactive chlorine in the northern hemisphere stratosphere, *Science*, *261*, 1134–1136, 1993.

Valdez, M. P., and G. A. Dawson, Sulfur dioxide incorporation into ice depositing from the vapor, *J. Geophys. Res.*, *94*(D1), 1095–1103, 1989.

Valdez, M. P., D. A. Standly, and G. A. Dawson, Gaseous deposition to snow: 1. Experimental study of SO_2 and NO_2 deposition, *J. Geophys. Res.*, *92*(D8), 9779–9787, 1987.

Varekamp, J. C., J. F. Luhr, and J. L. Prestegaard, The 1982 eruptions of El Chichón Volcano (Chiapas Mexico): Character of the eruptions, ash-fall deposits, and gasphase, *J. Volcanol. Geotherm. Res.*, *23*, 39–68, 1984.

Voisin, D., M. Legrand, and N. Chaumerliac, Scavenging of acidic gases (HCOOH, CH_3COOH, HNO_3, HCl, and SO_2) and ammonia in mixed liquid-solid water clouds at the Puy de Dome mountain (France), *J. Geophys. Res.*, *105*(D5), 6817–6835, 2000.

Wagnon, P., R. J. Delmas, and M. Legrand, Loss of volatile acid species from upper firn layers at Vostok, Antarctica, *J. Geophys. Res.*, *104*(D3), 3423–3431, 1999.

Walko, R. L., W. R. Cotton, M. P. Meyers, and J. Y. Harrington, New RAMS cloud microphysics parameterization. part I: The single moment scheme, *Atmos. Res.*, *38*, 29–62, 1995.

Wallace, L., and W. Livingston, The effect of the Pinatubo cloud on hydrogen chloride and hydrogen fluoride, *Geophys. Res. Lett.*, *19*(12), 1209, 1992.

Waters, J. W., L. Froidvaux, W. G. Read, G. L. Manney, L. S. Elson, D. A. Flower, R. F. Jarnot, and R. S. Harwood, Stratospheric ClO and ozone from the Microwave Lamb Sounder on the Upper Atmosphere Research Satellite, *Nature*, *362*, 597–602, 1993.

Westrich, H. R., and T. M. Gerlach, Magmatic gas source for the stratospheric SO_2 cloud from the June 15, 1991, eruption of Mount Pinatubo, *Geology*, *20*, 867–870, 1992.

Woods, A. W., The fluid dynamics and thermodynamics of eruption columns, *B. Volcanol.*, *50*, 169–193, 1988.

Woods, A. W., and S. Bower, The decompression of volcanic jets in craters, *Earth Planet. Sci. Lett.*, *131*, 189–205, 1995.

Woods, D. C., R. L. Chuan, and W. I. Rose, Halite particles injected into the stratosphere by the 1982 El Chichón eruption, *Science*, *230*, 170–172, 1985.

Yu, T., and W. I. Rose, Retrieval of sulfate and silicate ash masses in young (1–4 days old) eruption clouds using multiband infrared HIRS/2 data, in *Remote Sensing of Active Volcanism*, *Geophys. Monogr. Ser.*, vol. 116, edited by J. C. P. Mouginis-Mark, J. A. Crisp, and J. Fink, pp. 87–100, AGU, Washington, D.C., 2000.

Zdanowicz, C. M., G. A. Zielinski, and M. S. Germani, Mount Mazama eruption: Calendrical age verified and atmospheric impact assessed, *Geology*, *27*(7), 621–624, 1999.

H.-F. Graf, Max-Planck-Institut für Meteorologie, Bundesstrasse 55, D-20146 Hamburg, Germany. (graf@dkrz.de)

M. Herzog, Department of Atmospheric, Oceanic and Space Sciences, University of Michigan, 2455 Hayward, Ann Arbor, MI 48109-2143, USA. (herzogm@engin.umich.edu)

J. M. Oberhuber, Deutsches Klimarechenzentrum GmbH, Bundesstrasse 55, D-20146 Hamburg, Germany.

C. Textor, Laboratoire des Sciences du Climat et de l'Environnement, Orme des Merisiers, F-91191 Gif-sur-Yvette, France. (textor@lsce.saclay.cea.fr)